S1. Experimental Section.

S1.1. Materials

Citric acid was purchased from Heowns Co., Ltd. Yttrium oxide (Y_2O_3, 99%) was purchased from Shanghai Yuanye Bio-Technology Co., Ltd. The commercial 8-MR (eight-membered-ring) zeolites/zeo-type materials SSZ-39, SSZ-13, and CCG-MTO materials were obtained from China Catalyst Group (CCG) Holding CO., Ltd. The zeo-type SAPO-34 was obtained from Nankai University Catalyst Co., Ltd. SAPO-18 was purchased from Raodong Co., Ltd. All commercial zeolites were dried at 120 °C for 12 h and then calcined at 550 °C for 6 h to remove the residual synthesis template for future using.

S1.2. Catalyst preparation.

S1.2.1. Preparation of etching samples.

A series of etching zeolites were prepared by etching the commercial 8-MR zeolites/zeo-type materials with citric acid solutions of different concentrations, as also previously reported in the literature.[1–4] The commercial 8MR zeolites and the different concentrations of citric acid solution were mixed at a mass ratio of 1:20, and then the mixture was stirred at 70 °C for 2h. After citric acid treatment, the obtained samples were filtered and washed with deionized water, subsequently dried at 100 °C for 12h, and calcined at 500 °C for 4h. The treated samples were named “zeolite (SAPO-34, SAPO-18, CCG-MTO, SSZ-13, SSZ-39)-etching” in this study, while sometimes the concentration was also mentioned (like zeolite-etching-xM CA, where x represents citric acid concentrations).

S1.2.2. Preparation of steamed samples.

The commercial 8MR zeolites (3.0g) were loaded in a fixed-bed quartz tubular reactor with an inner diameter of 8 mm under atmospheric pressure. The furnace was ramped at 1°C/min to 750 °C and held there for 8h. The furnace was fed a flow of helium-created bubbling zero-grade helium over 100cc/min through a water saturator heated at 120 °C through the whole heating process, including ramping up and cooling down.[5–7] The treated samples were named as "zeolites (SAPO-34, SAPO-18, CCG-MTO, SSZ-13, SSZ-39)-ST750" in this study.

S1.3. Catalyst characterization.

Powder X-ray diffraction (XRD) patterns were measured on a Bruker D8 Advance X-ray diffractometer with Cu Kα radiation. The data were collected in the 2θ range of 5–70° with a step size of 0.02°. Scanning electron microscopy (SEM) imaging was obtained by Hitachi-SU8010, Japan. Temperature-programmed NH_3 desorption (NH_3-TPD) was measured by Micromeritics AutoChem II 2920. ~50 mg of sample was used for the test in a 30 mL min^{-1} Ar flow. Prior to the test, the sample was heated to 550 °C and kept for 60 min to remove possible impurities. Afterward, the sample was cooled to 100 °C and exposed to a 30 mL min^{-1} NH_3 flow for 1h to saturate the surface completely, which was followed by purging with a 30 mL min^{-1} ultrahigh purity He flows to remove any physically adsorbed NH_3 for 30 min. After all these pretreatments, the catalyst was heated from 100 °C to 700 °C at a rate of 10 °C min^{-1}**.** ^{27}Al MAS solid-state NMR experiments were carried out on 400 MHz Bruker AVANCE IV 21.1T spectrometers equipped with 3.2 mm CPMAS probes, where chemical shifts were externally referenced to $Al(NO_3)_3$. All NMR spectra were processed and analyzed using Bruker TopSpin

4.0. The specific surface area and pore volume of zeolites were obtained by N_2 physisorption at −196 °C on a Micromeritics ASAP 2460 instrument. The samples were outgassed at 350 °C for 8h before the sorption measurements. The total specific surface area was determined after using the BET method, while the external surface area and micropore volume were derived from the t-plot method. The total pore volume was derived from a single-point measurement at P/P_0 = 0.99. The coke deposition on spent zeolites was determined via thermal gravimetric analysis (TGA) using a STA 449 F3 Jupiter® instrument manufactured by NETZSCH, Germany. Typically, 10 mg of spent zeolites were heated under argon atmosphere at 10°C/min to 100°C, held for 30 minutes to remove surface adsorbed moisture, cooled to room temperature, and then heated at 10°C/min to 850°C under an airflow of 30 ml/min. Quantitative compositional analysis of untreated and treated zeolites was performed using Thermo Fisher Scientific's ARL Advant X IntellipowerTM 3600 equipment, utilizing X-ray fluorescence spectroscopy (XRF).

S1.4. Catalytic evaluation.

The methanol-to-olefins (MTO) reaction was performed in a fixed-bed quartz tubular reactor (Xiamen Hande Engineering Co., Ltd.) with an inner diameter of 10 mm under atmospheric pressure. Firstly, the 8-MR zeolites/zeo-type materials were pelletized and sieved to 25-40 mesh for future use. Prior to the reaction, 0.5 g catalytic material mixed with 3.0 g SiC was loaded in a fixed-bed quartz tubular reactor heated to 400 °C using argon as the carrier gas with a flow rate of 11.7 ml/min for 1 h. For the untreated 8MR zeolites, prior to the reaction, were heated to 550 °C using argon as the carrier gas with a flow rate of 11.7 ml/min for 2h,

then cooled down to the reaction temperature. The treated or dealuminated catalytic materials underwent pre-treatment at the same temperature as the reaction temperature to avoid realumination upon heating at higher temperatures. After the pre-treatment, methanol was fed into the fixed bed reactor by the carrier gas of argon, corresponding to a weight hourly space velocity of 1.0/h. Intra-mixed samples were prepared by physically mixing zeolite powders with Y_2O_3 powders using an agate mortar and pestle and pelletizing, crushing, and sieving to obtain 25-40 mesh aggregates. Inter-mixed mixtures were prepared by mixing individually prepared 25-40 mesh aggregates of zeolites with 25-40 mesh aggregates of Y_2O_3. All the mass ratio of zeolite/Y_2O_3 was 1:1.[8–10] The reaction products were analyzed online using gas chromatography (GC-8850, Lunan Ruihong Co., Ltd.) with three detectors: two flame ionization detectors (FIDs) and one thermal conductivity detector (TCD). The permanent gas (Ar, N_2, CH_4, CO, and CO_2) was detected by TCD through GDX-104 and TDX-101 columns. The separation of methanol, dimethoxy ether (DME), and C1−C4 hydrocarbons was carried out on a KB-PLOT Q column (30m*0.53mm*40um), while the separation of C5+ hydrocarbons was carried out on a KB-5 column (60m*0.32mm*1.0um). Methanol conversion (X, %) and products selectivity (S, %) are defined as follows:

$$X\% = \frac{n_{C,MeOH_{in}} - n_{C,MeOH_{out}} - 2n_{C,DME_{out}}}{n_{C,MeOH_{in}}} \quad (1)$$

$$S_i\% = \frac{i * n_{Ci}}{n_{C,MeOH_{in}} - n_{C,oxy_{out}}} \quad (2)$$

Where $n_{C,MeOHin}$, $n_{C,MeOHout}$, are the concentrations determined by GC analysis of methanol in the blank and in the reactor effluent. $n_{C,DMEout}$ and $n_{C,oxyout}$ are the concentrations of DME and oxygenates in the effluents, n_{Ci} is the concentration of the reactor effluent determined by GC analysis of a product with n carbon atoms.

S1.5. Operando UV-Vis Diffuse Reflectance Spectroscopy (DRS) Study Coupled with Online Mass Spectrometry (MS)

All the catalytic operando studies were performed using a Linkam cell (THMS600) equipped with a temperature controller (Linkam TMS94), and its lid is equipped with a quartz window compatible with UV/Vis detection. The UV/Vis diffuse reflectance spectroscopy (DRS) measurements were performed with an AvaSpec-ULS2048L-USB2-UA-RS microspectrophotometer from Avantes. Halogen and deuterium lamps were used together for illumination. The online gas phase product analyses were performed by Pfeiffer OmniStar GSD 350 O3 (1-200 amu) mass spectrometer, which was directly connected to the outlet of the Linkam cell. The National Institute of Standards and Technology (NIST) mass spectrometry database was consulted for assignment and referencing purposes. Herein, the signals identified at 26 amu, 41 amu, 56 amu and 70 amu were attributed to ethylene, propylene, butene and pentene, respectively. During operando studies, all reactions were performed without pressing and sieving the zeolite materials. Operando UV/Vis DRS reactions were performed using ca. 40 mg of the catalyst material. Initially, it was placed on the heating stage of the Linkam cell, which was further connected to a water cooler. The inlet of the cell was connected to the N_2 gas line, via a liquid saturator, whereas the outlet was either connected to the Pfeiffer mass spectrometer or vented out. The lid of the Linkam cell is equipped with a quartz window to monitor the reaction by UV-vis DRS. Before each UV-vis DRS, the material was further pre-treated/calcined according to the following procedure under an N_2 environment (flow rate of 20 ml/min): heating to 400 °C at 10 °C /min and keeping the sample at this temperature for the

next 10min; then, heating the sample to 550 °C at a rate of 5 °C /min and hold there for the next 30 min. Next, the sample was cooled down to the reaction temperature (as specified in the Fig. caption) with a rate of 10 °C/min under a flow of N_2 gas (flow rate of 20 ml/min). For treated/dealuminated 8MR zeolites, under an N_2 environment (flow rate of 20 ml/min), heating to 400 °C at 10 °C /min and keeping the sample at this temperature for testing. The starting time of the reaction was considered to be when the inward N_2 flow went through the liquid saturator. Finally, the reaction was quenched by rapid cooling of the Linkam cell using a Linkam TMS94 temperature controller. During these experiments, the UV-vis DRS was recorded every 15 seconds during the MTO experiment, which typically took 40 minutes. The Operando UV-vis spectra were collected every minute, with 300 accumulations of 50 ms exposure time each.

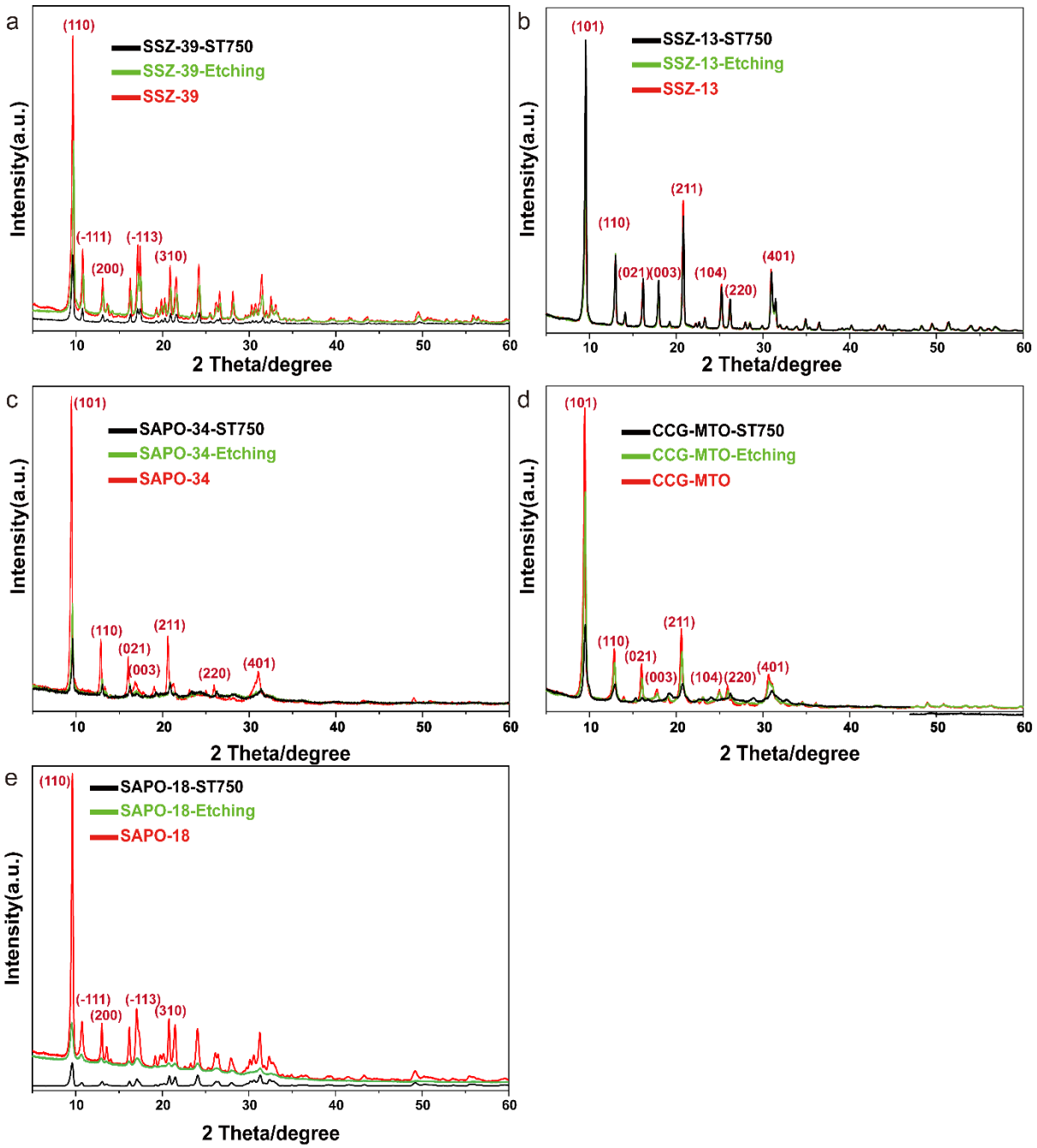

Fig. S1 X-ray diffraction patterns of untreated and dealuminated (a) SSZ-39, (b) SSZ-13, (c) SAPO-34, (d) CCG-MTO, and (e) SAPO-18 zeolites/zeo-type materials.

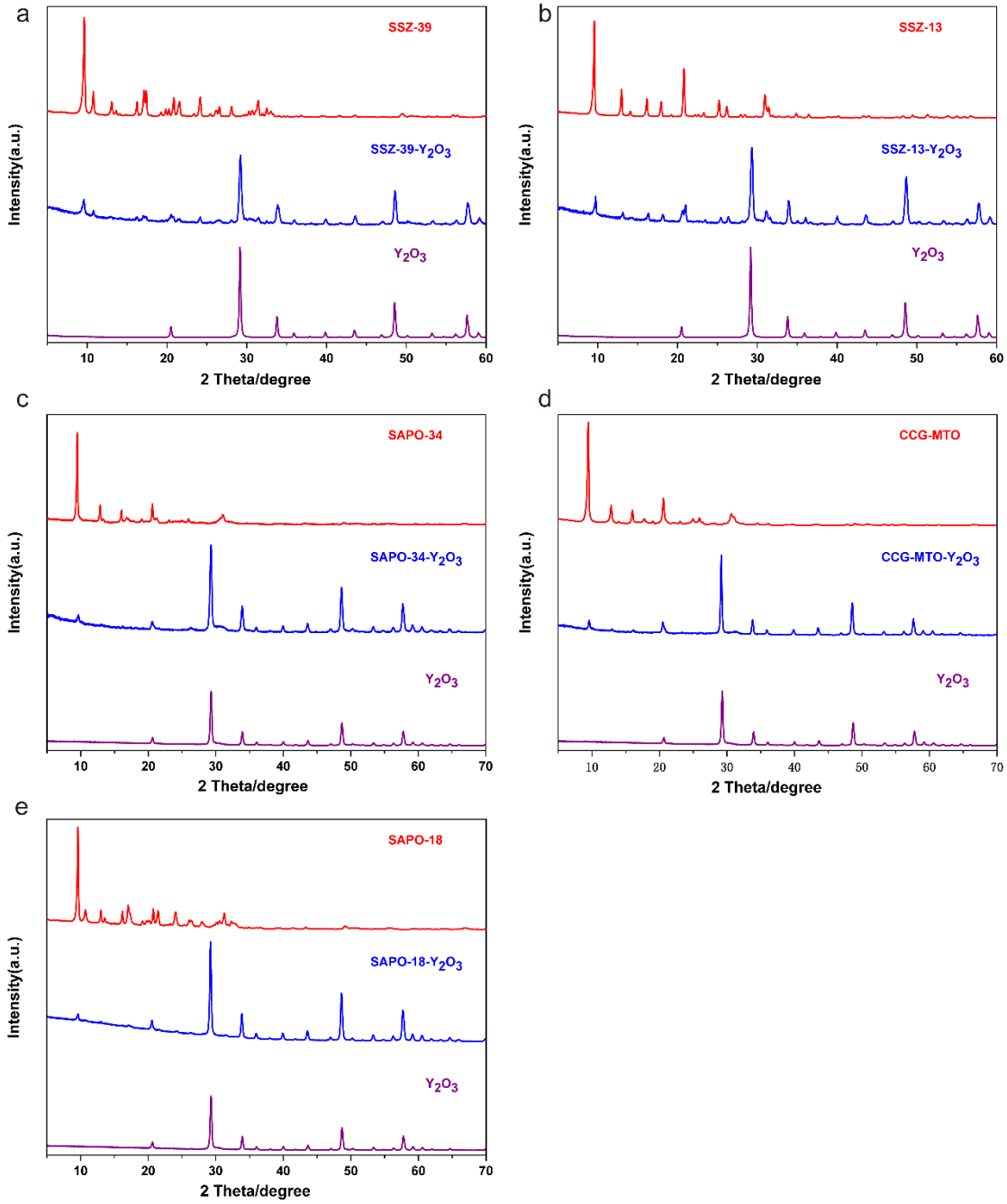

Fig. S2 X-ray diffraction patterns of the bifunctional catalytic systems based on Y_2O_3 and parent (a) SSZ-39, (b) SSZ-13, (c) SAPO-34, (d) CCG-MTO, and (e) SAPO-18 zeolites/zeo-type materials. After mixing commercial zeolites with Y_2O_3, the resulting XRD patterns overwhelmingly retained the peak shape of Y_2O_3 and a small portion of the zeolite peak shape, without any other impure peak shape observed, suggesting that the mixtures may have been prepared via physical methods.

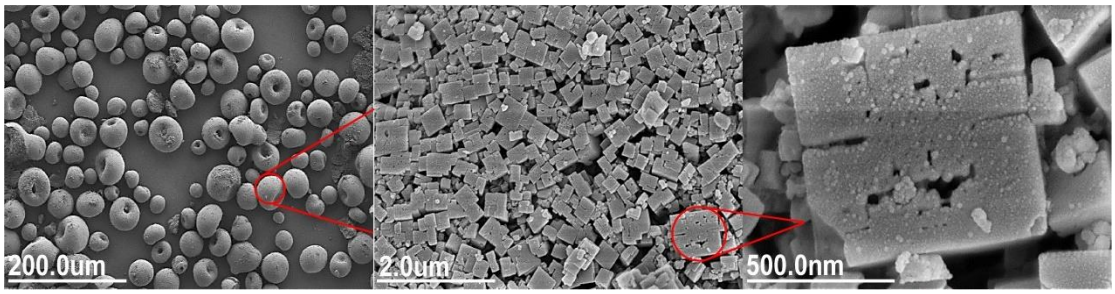

Fig. S3 SEM images of the industrial CCG-MTO material.

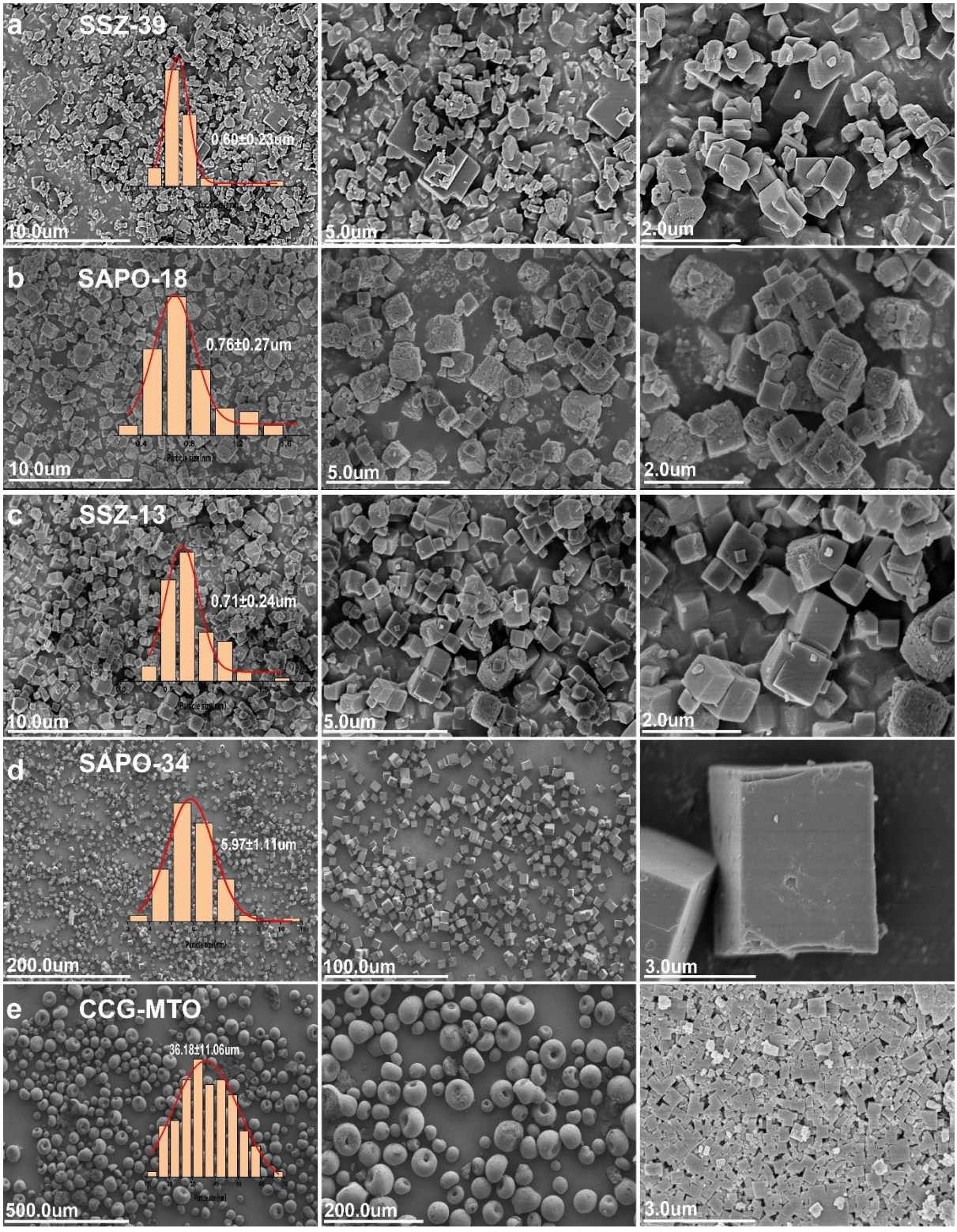

Fig. S4 SEM images of parent and untreated (a) SSZ-39, (b) SAPO-18, (c) SSZ-13, (d) SAPO-34, (e) CCG-MTO zeolites/zeo-type materials.

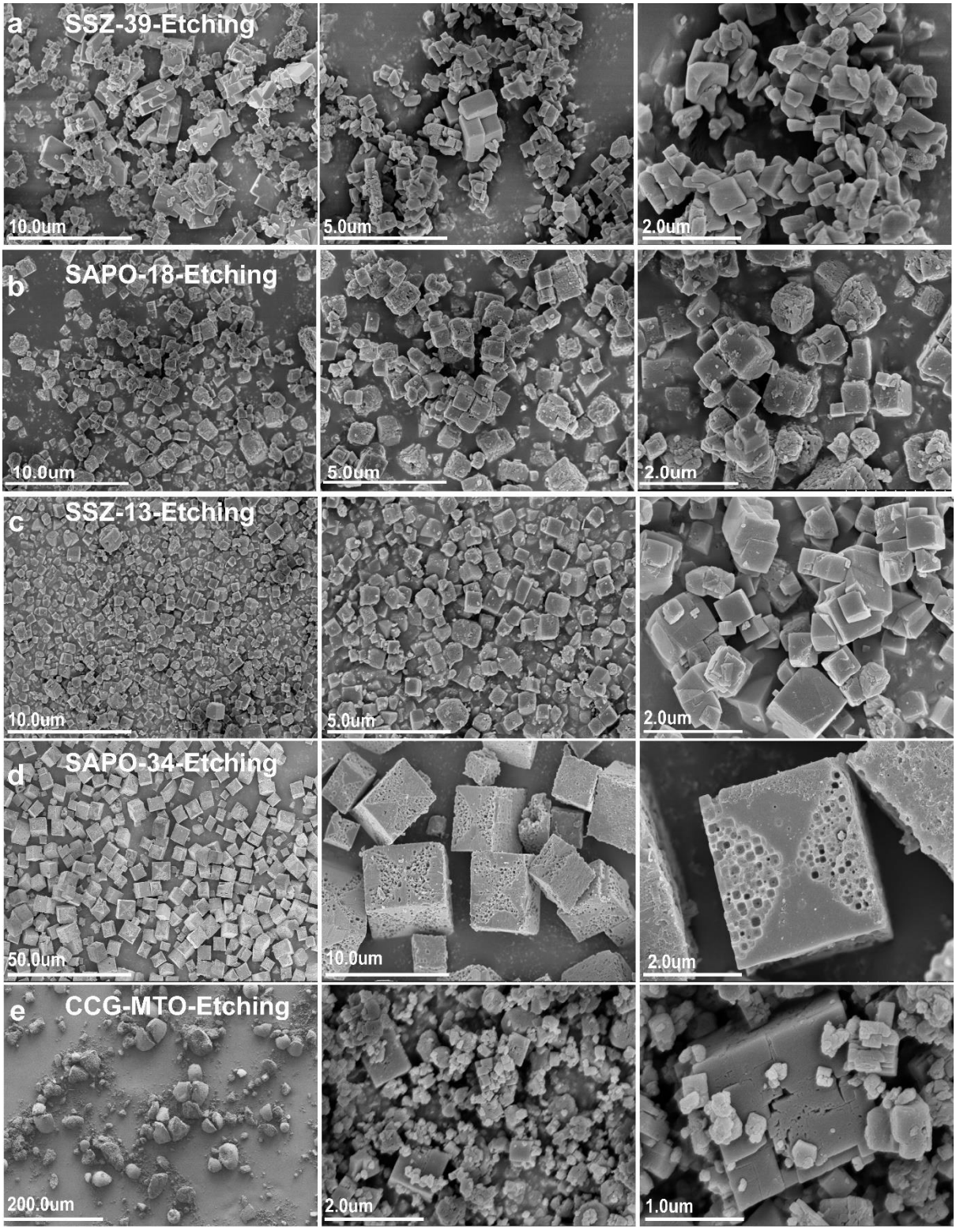

Fig. S5 SEM images of chemical etching (a) SSZ-39, (b) SAPO-18, (c) SSZ-13, (d) SAPO-34, (e) CCG-MTO zeolites/zeo-type materials.

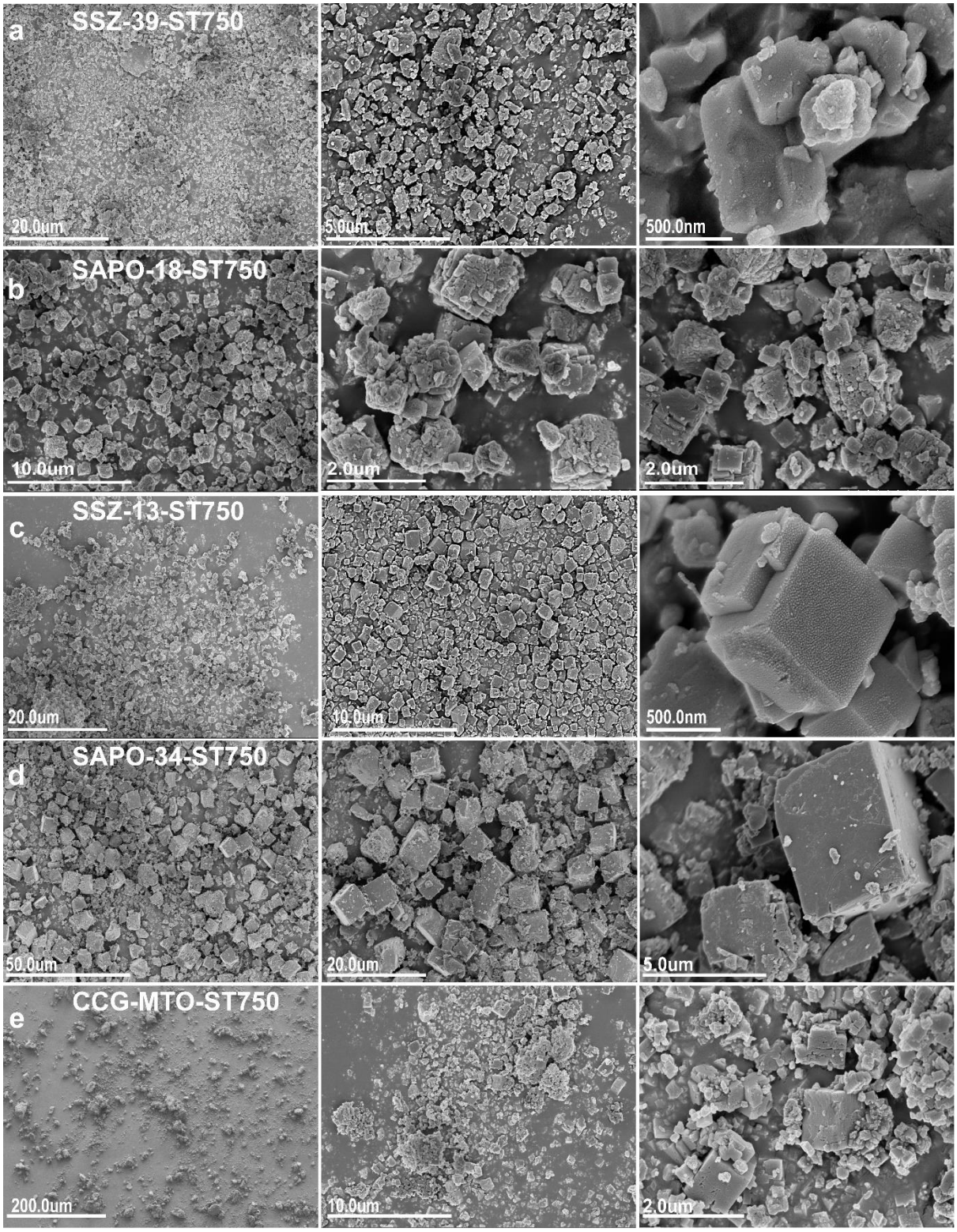

Fig. S6 SEM images of steamed (a) SSZ-39, (b) SAPO-18, (c) SSZ-13, (d) SAPO-34, (e) CCG-MTO zeolites/zeo-type materials.

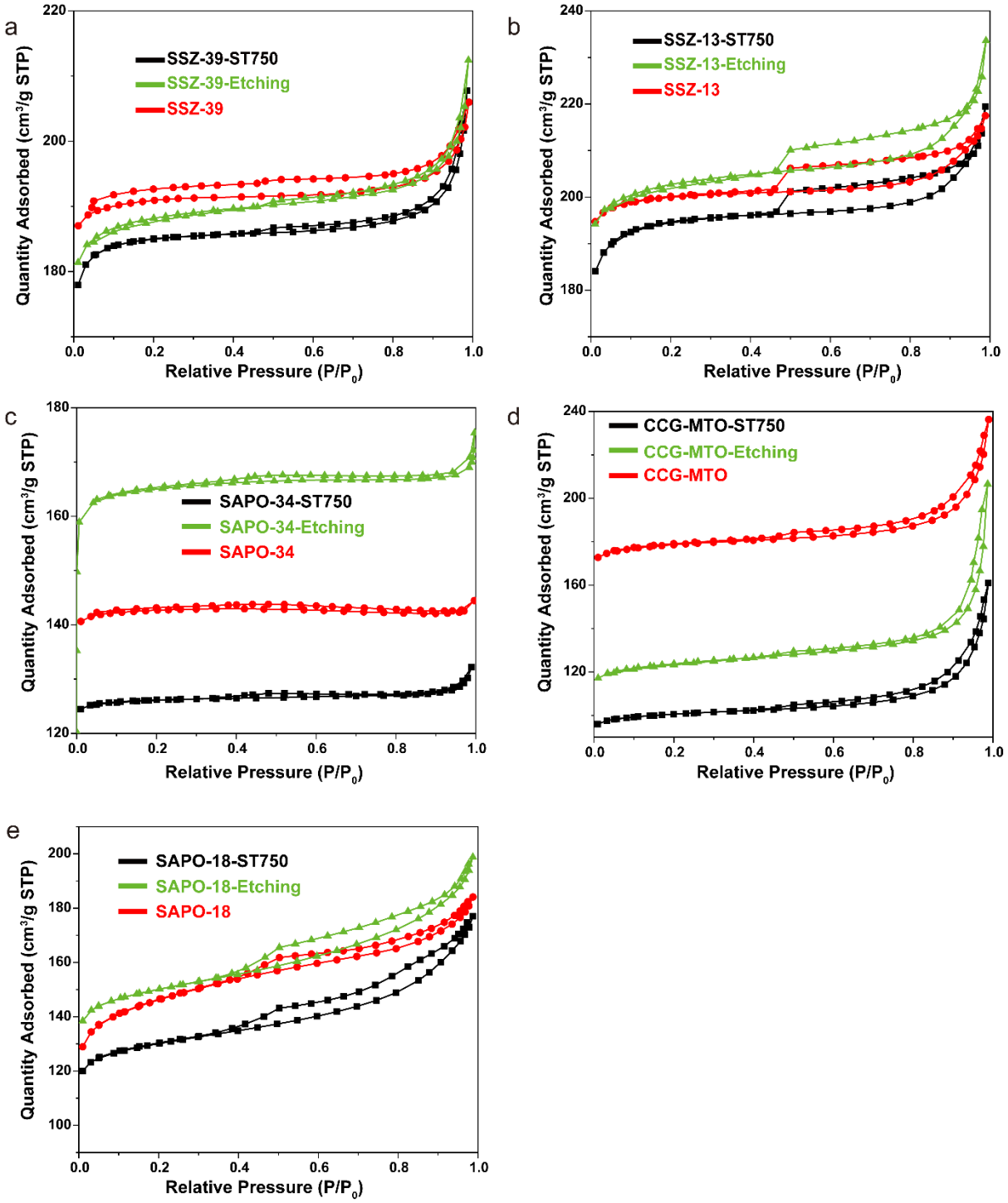

Fig. S7 N_2 physisorption isotherms of untreated and dealuminated (a) SSZ-39, (b) SSZ-13, (c) SAPO-34, and (d) CCG-MTO, and (e) SAPO-18 zeolites/zeo-type materials.

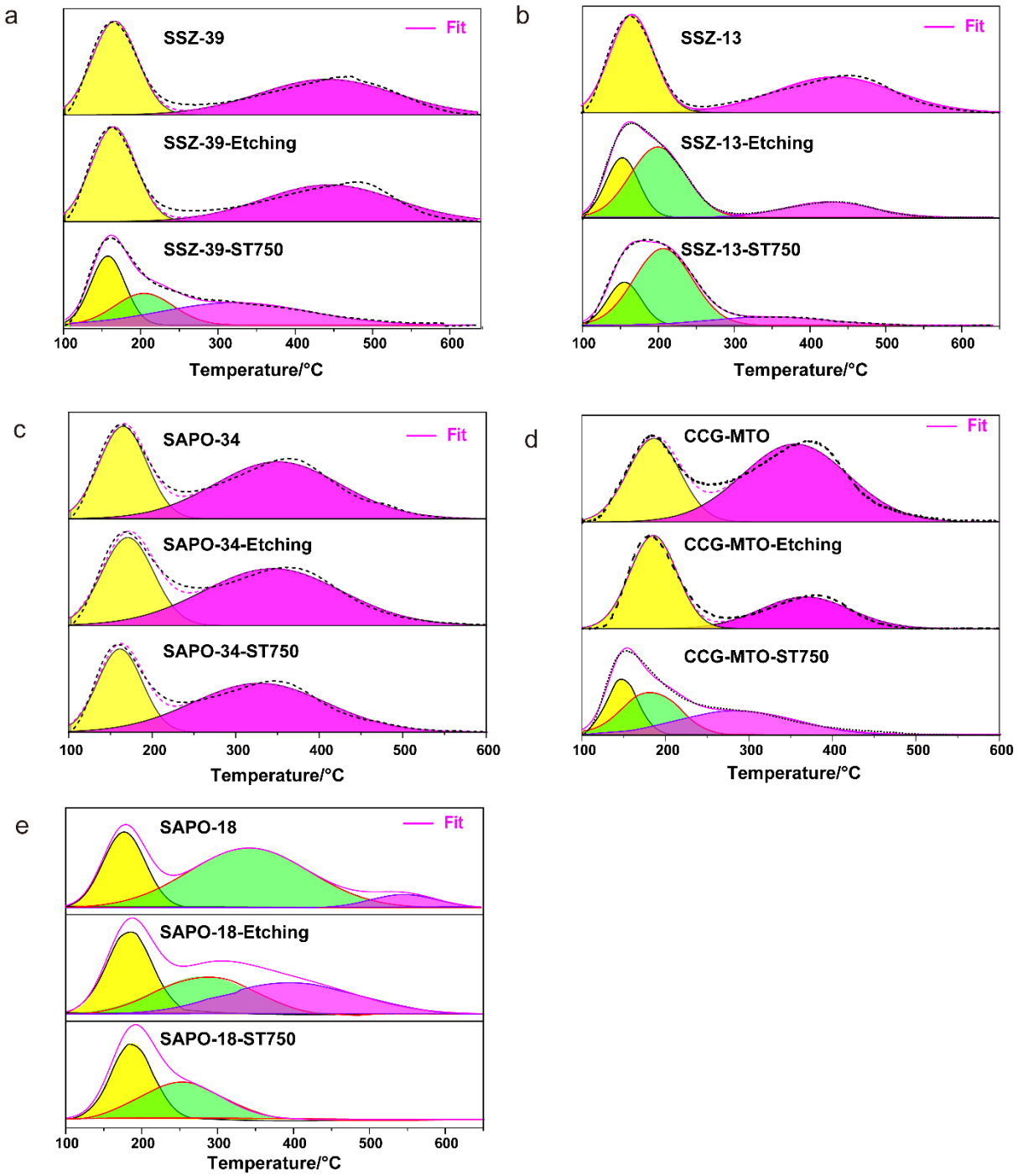

Fig. S8 NH_3-TPD profiles of untreated and dealuminated (a) SSZ-39, (b) SSZ-13, (c) SAPO-34, (d) CCG-MTO, and (e) SAPO-18 zeolites/zeo-type materials.

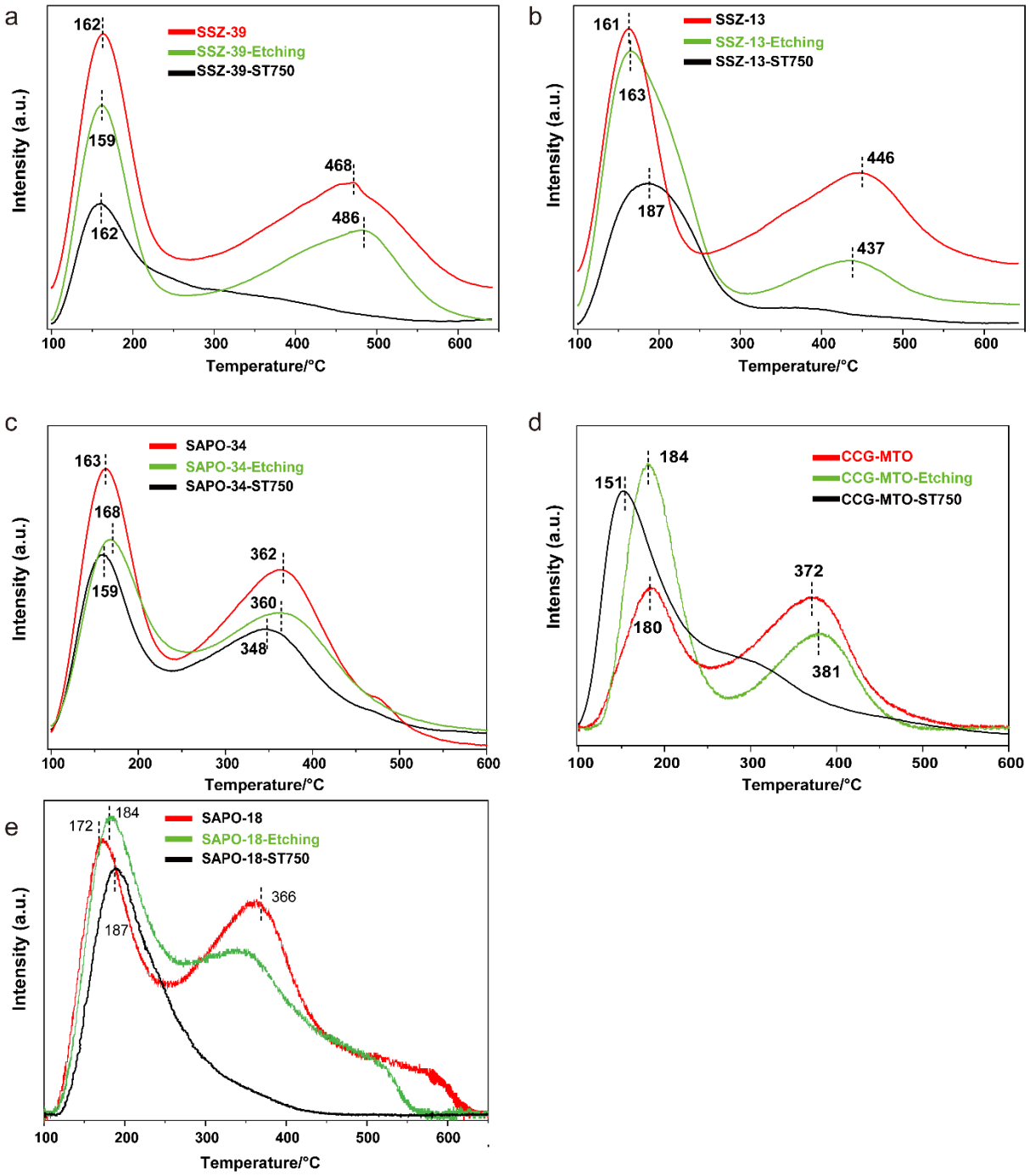

Fig. S9 NH_3-TPD profiles of untreated and dealuminated (a) SSZ-39, (b) SSZ-13, (c) SAPO-34, (d) CCG-MTO, and (e) SAPO-18 zeolites/zeo-type materials.

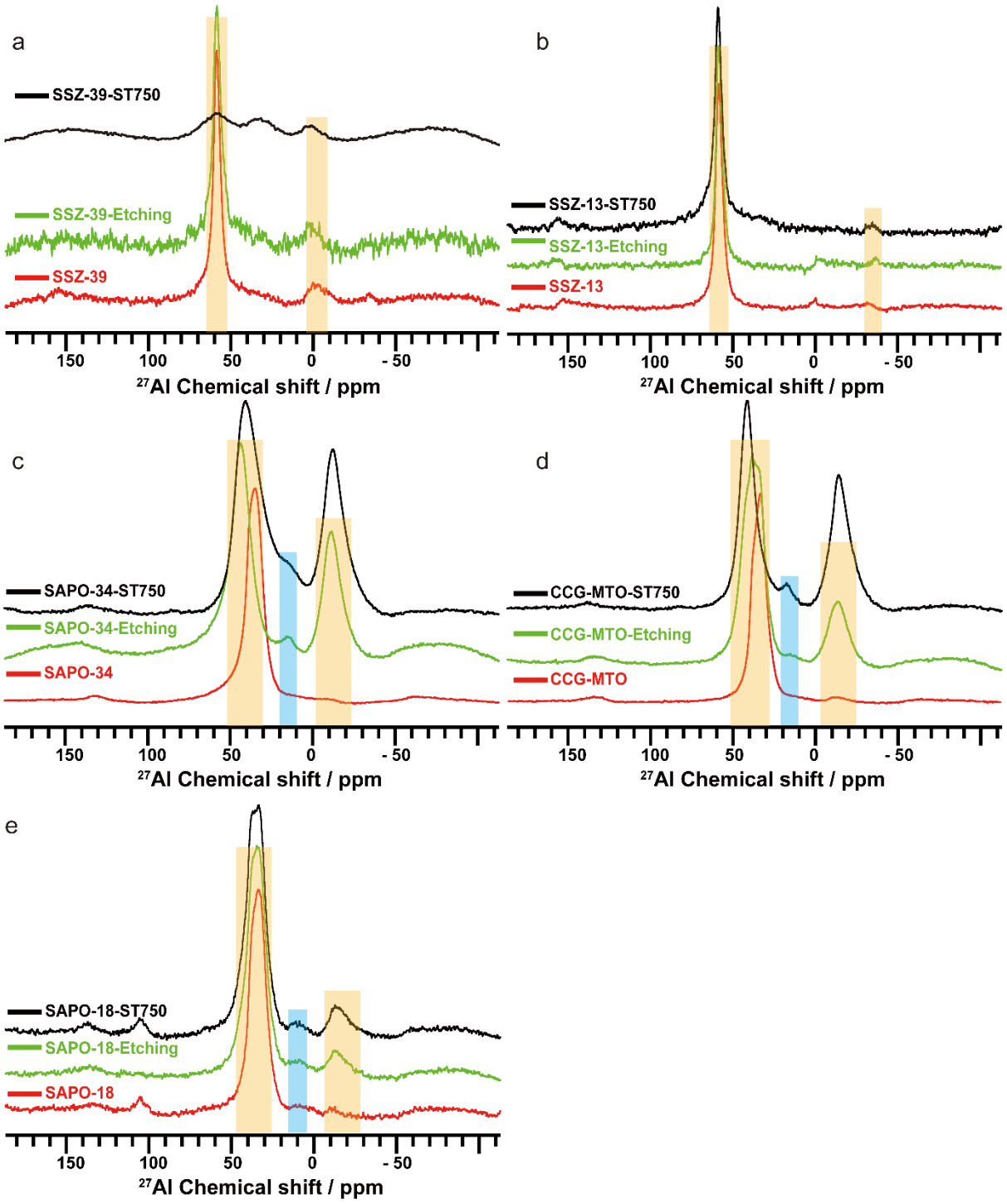

Fig. S10 ^{27}Al MAS NMR spectra of standalone untreated zeolites/zeo-type materials and their dealuminated forms after the steaming and chemical etching treatments: (a) SSZ-39, (b) SSZ-13, (c) SAPO-34, (d) CCG-MTO and (e) SAPO-18 zeolites/zeo-type materials. For the SSZ-39-ST750 material, the number of scans (NS) value was 10K, while NS=2k for other materials.

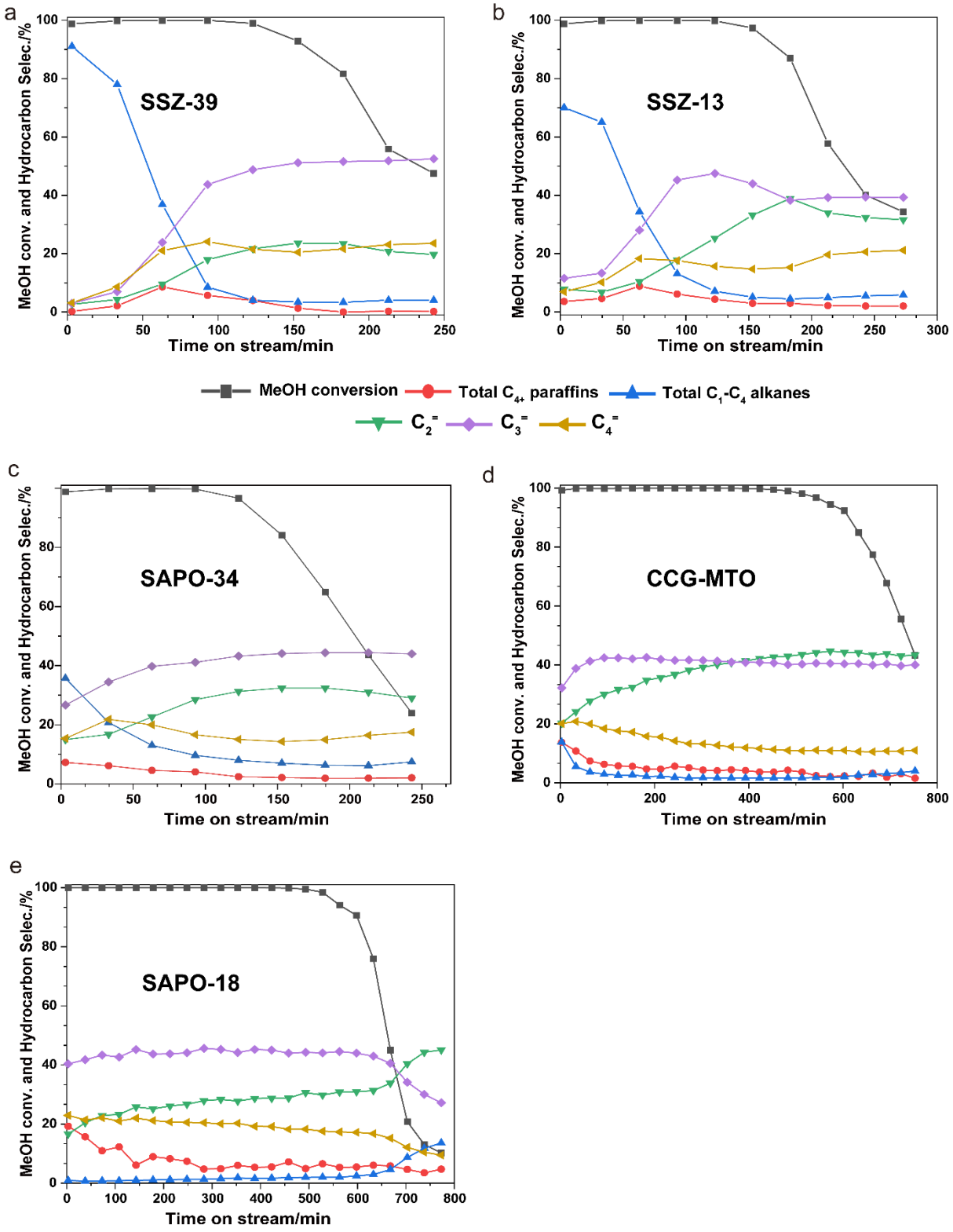

Fig. S11 Catalytic data of methanol conversion and hydrocarbon selectivity of parent (a) SSZ-39, (b) SSZ-13, (c) SAPO-34, (d) CCG-MTO, and (e) SAPO-18 zeolites/zeo-type materials with respect to time-on-stream (TOS) (Reaction conditions: 400 °C, WHSV =1h^{-1}).

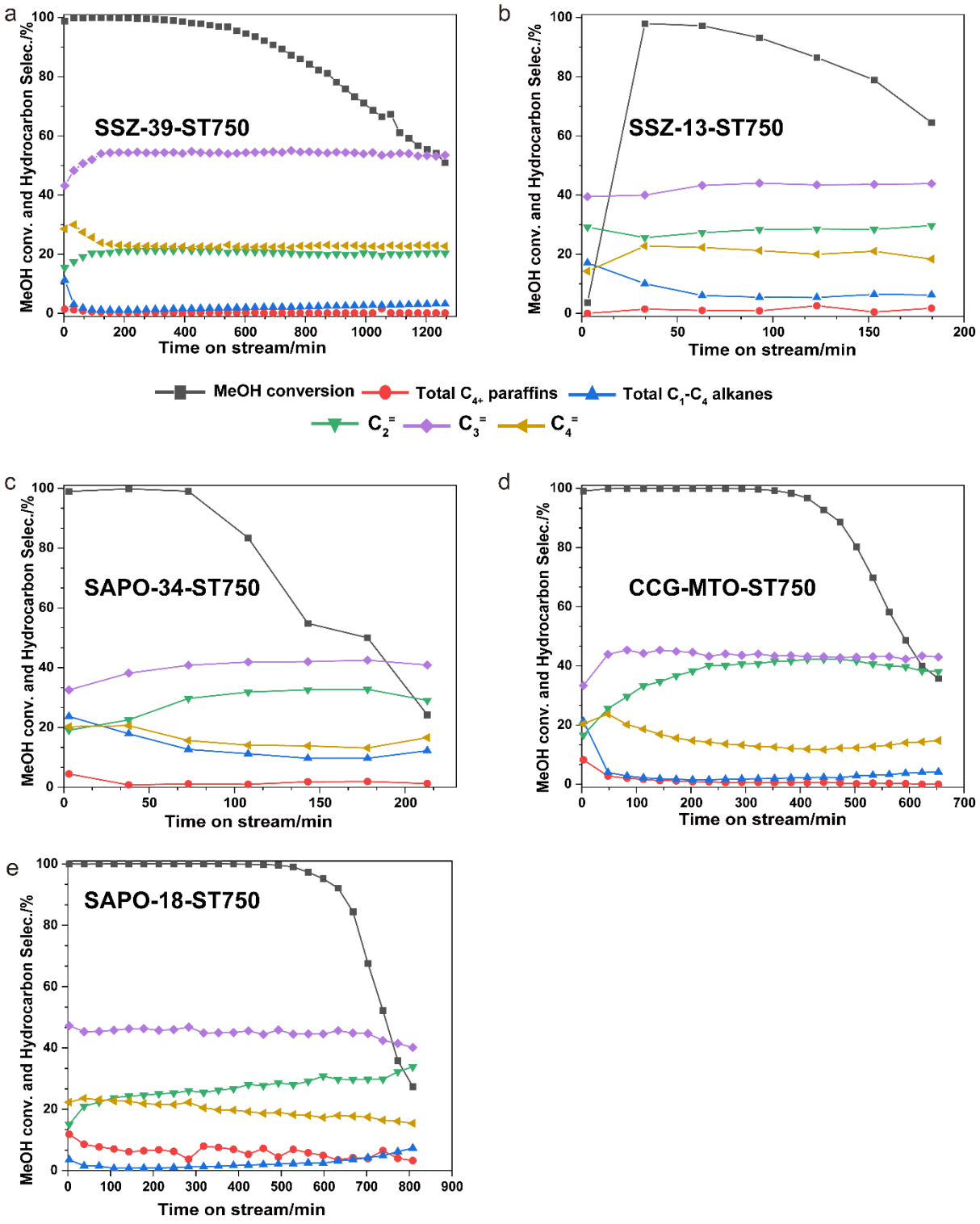

Fig. S12 Catalytic data of methanol conversion and hydrocarbon selectivity of steamed (a) SSZ-39, (b) SSZ-13, (c) SAPO-34, (d) CCG-MTO, and (e) SAPO-18 zeolites/zeo-type materials with respect to time-on-stream (TOS) (Reaction conditions:400 °C, WHSV=1h^{-1}).

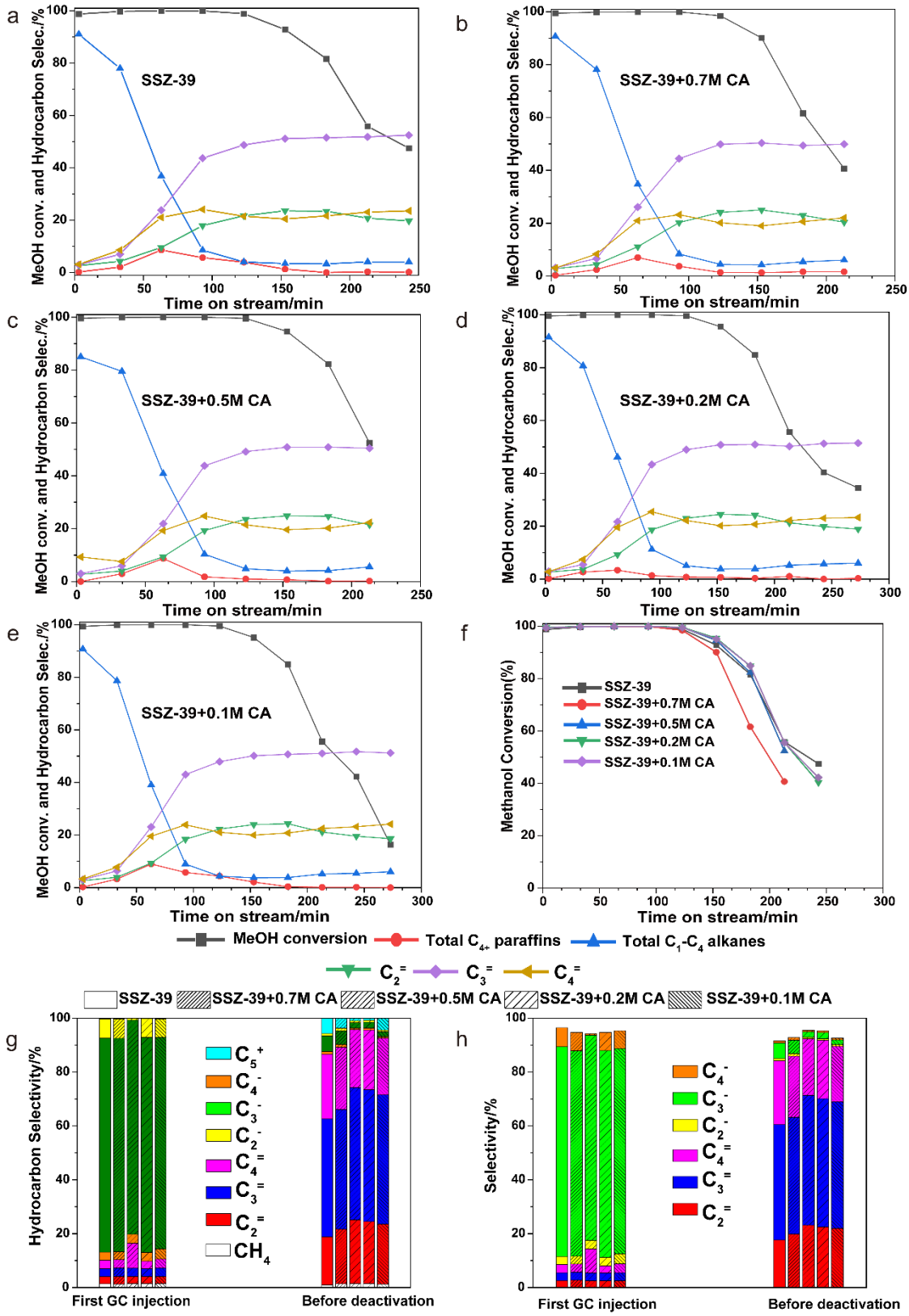

Fig. S13 Catalytic data of methanol conversion and hydrocarbon selectivity of chemically etching (a) SSZ-39, (b) SSZ-39-0.7M CA, (c) SSZ-39-0.5M CA, (d) SSZ-39-0.2M CA, and (e) SSZ-39-0.1M CA zeolite materials with respect to time-on-stream (TOS) (Reaction conditions: 400 °C, WHSV=1h^{-1}). The overlapping comparison of their (f) Methanol conversion along with (g-h) hydrocarbon/product selectivity (xM CA implies the citric acid concentration).

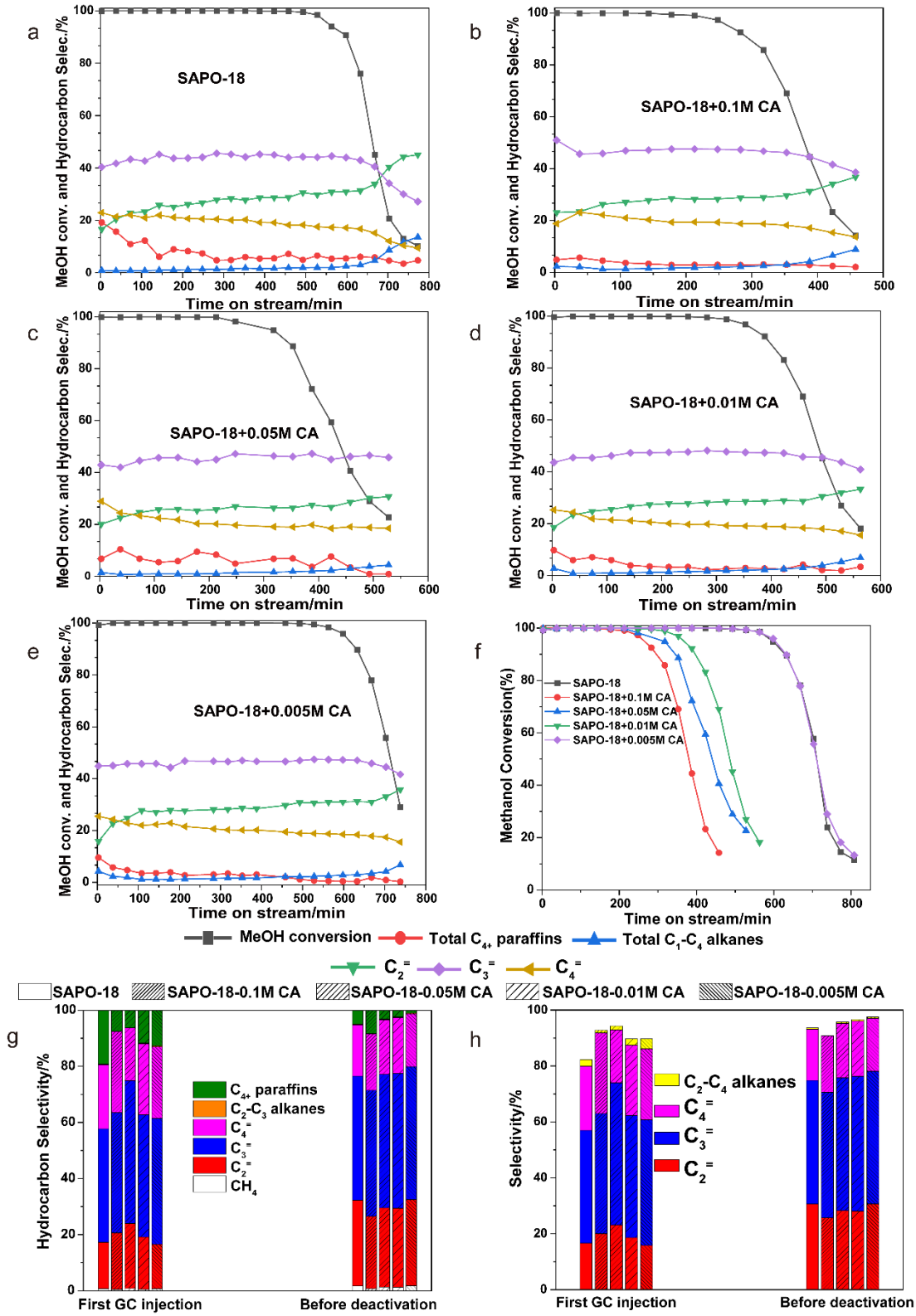

Fig. S14 Catalytic data of methanol conversion and hydrocarbon selectivity of chemically etching (a) SAPO-18, (b) SAPO-18-0.1M CA, (c) SAPO-18-0.05M CA, (d) SAPO-18-0.01M CA, and (e) SAPO-18-0.005M CA zeolite materials with respect to time-on-stream (TOS) (Reaction conditions: 400 °C, WHSV=1h^{-1}). The overlapping comparison of their (f) Methanol conversion along with (g-h) hydrocarbon/product selectivity (xM CA implies the citric acid concentration).

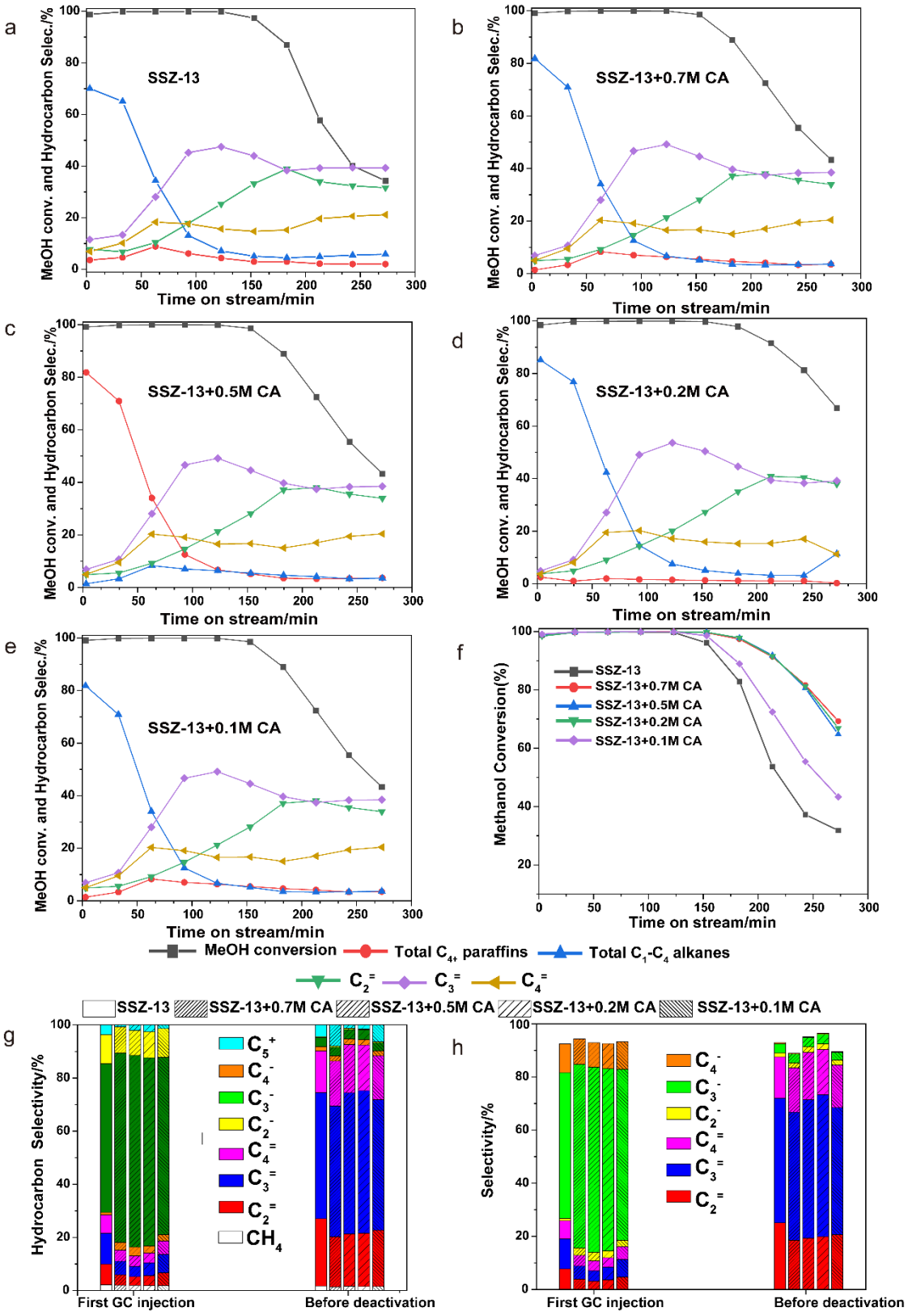

Fig. S15 Catalytic data of methanol conversion and hydrocarbon selectivity of chemically etching (a) SSZ-13, (b) SSZ-13-0.7M CA, (c) SSZ-13-0.5M CA, (d) SSZ-13-0.2M CA, (e) SSZ-13-0.1M CA zeolite materials with respect to time-on-stream (TOS) (Reaction conditions: 400 °C, WHSV=1h^{-1}). The overlapping comparison of their (f) Methanol conversion along with (g-h) hydrocarbon/product selectivity.

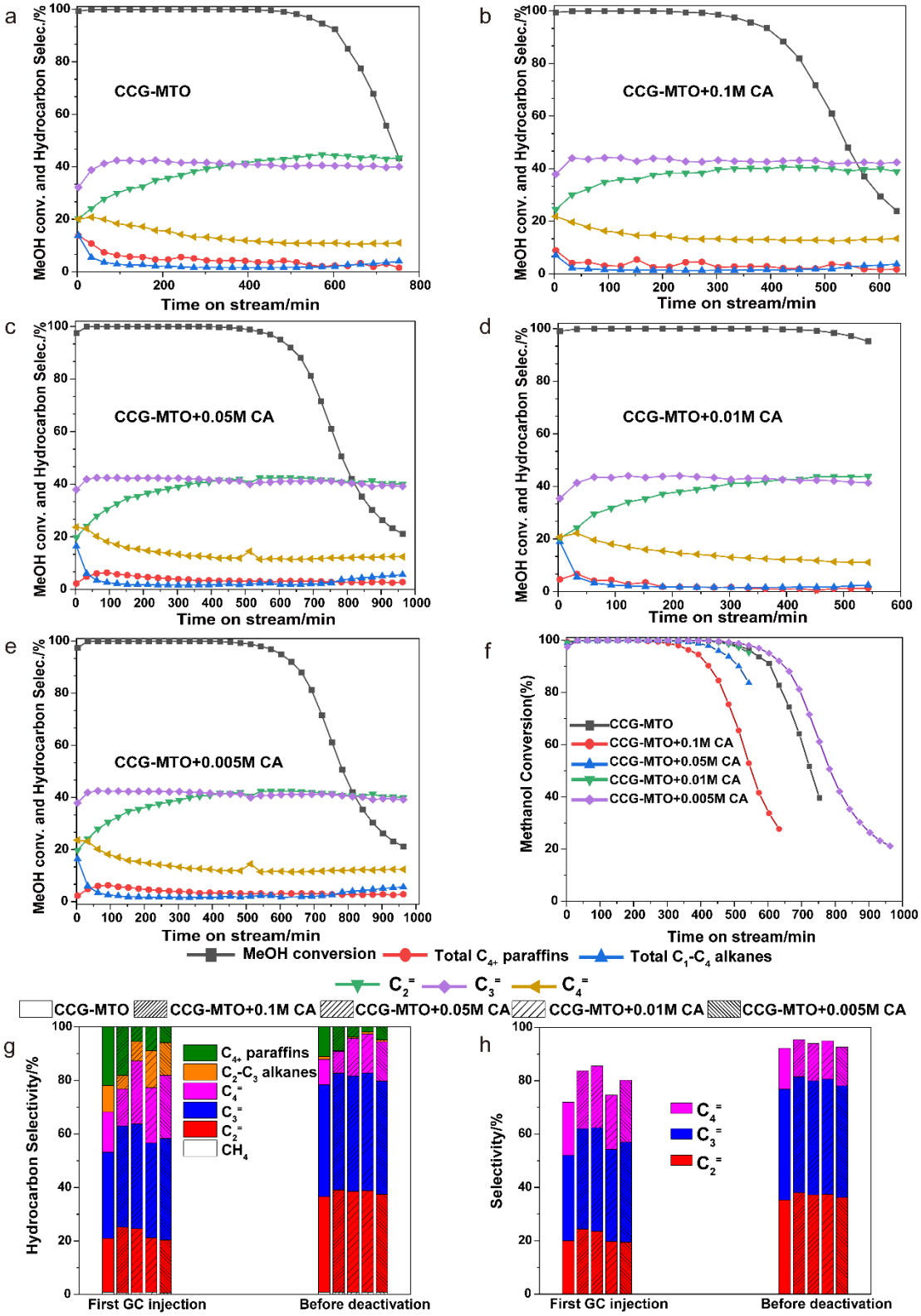

Fig. S16 Catalytic data of methanol conversion and hydrocarbon selectivity of chemically etching (a) SAPO-34, (b) SAPO-34-0.1M CA, and (c) SAPO-34-0.05M CA zeolite materials with respect to time-on-stream (TOS) (Reaction conditions: 400 °C, WHSV=1h^{-1}). The overlapping comparison of their (f) Methanol conversion along with (g-h) hydrocarbon/product selectivity (xM CA implies the citric acid concentration).

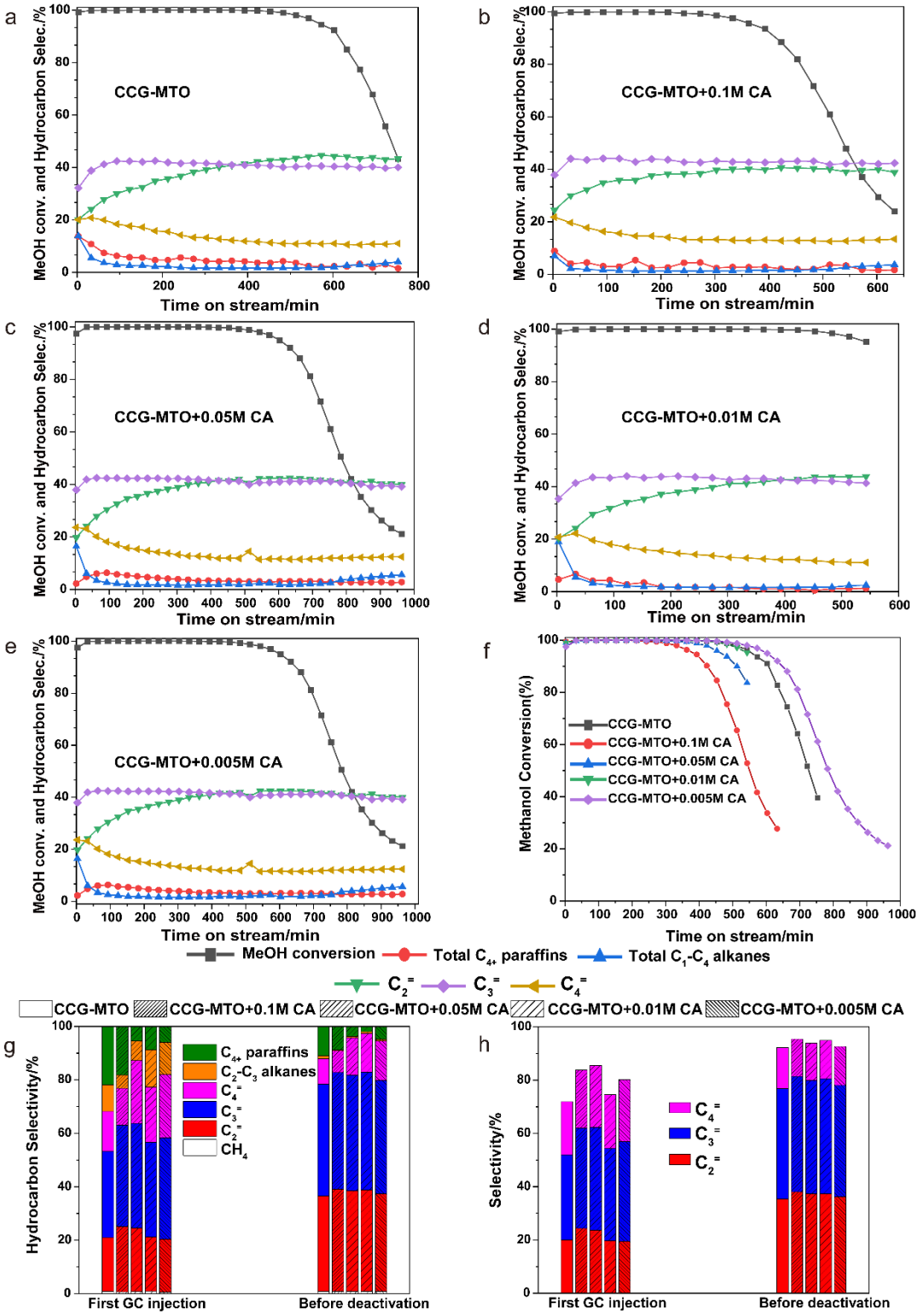

Fig. S17 Catalytic data of methanol conversion and hydrocarbon selectivity of etching (a) CCG-MTO, (b) CCG-MTO-0.1M CA, (c) CCG-MTO-0.05M CA, (d) CCG-MTO-0.01M CA, and (e) CCG-MTO-0.005M CA zeo-type materials with respect to time-on-stream (TOS) (Reaction conditions:400 °C, WHSV=1h^{-1}). The overlapping comparison of their (f) Methanol conversion along with (g-h) hydrocarbon/product selectivity (xM CA implies the citric acid concentration).

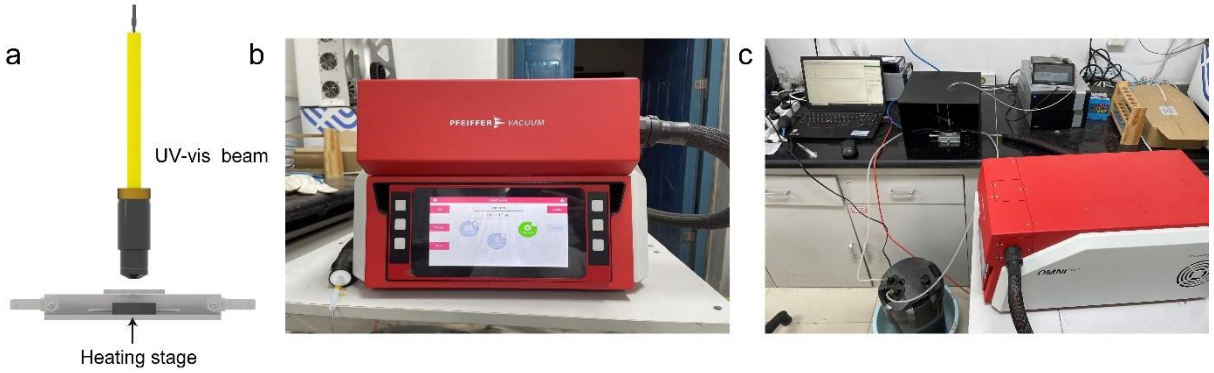

Fig. S18 The operando set-up consists of UV-Vis diffuse reflectance spectroscopy (UV-Vis DRS) coupled with online mass spectrometry (MS): (a) Illustration of the UV-vis DRS working principle along with images of (b) online MS, and (c) the whole working set-up. See experimental Section **S1.5.** for the technical details.

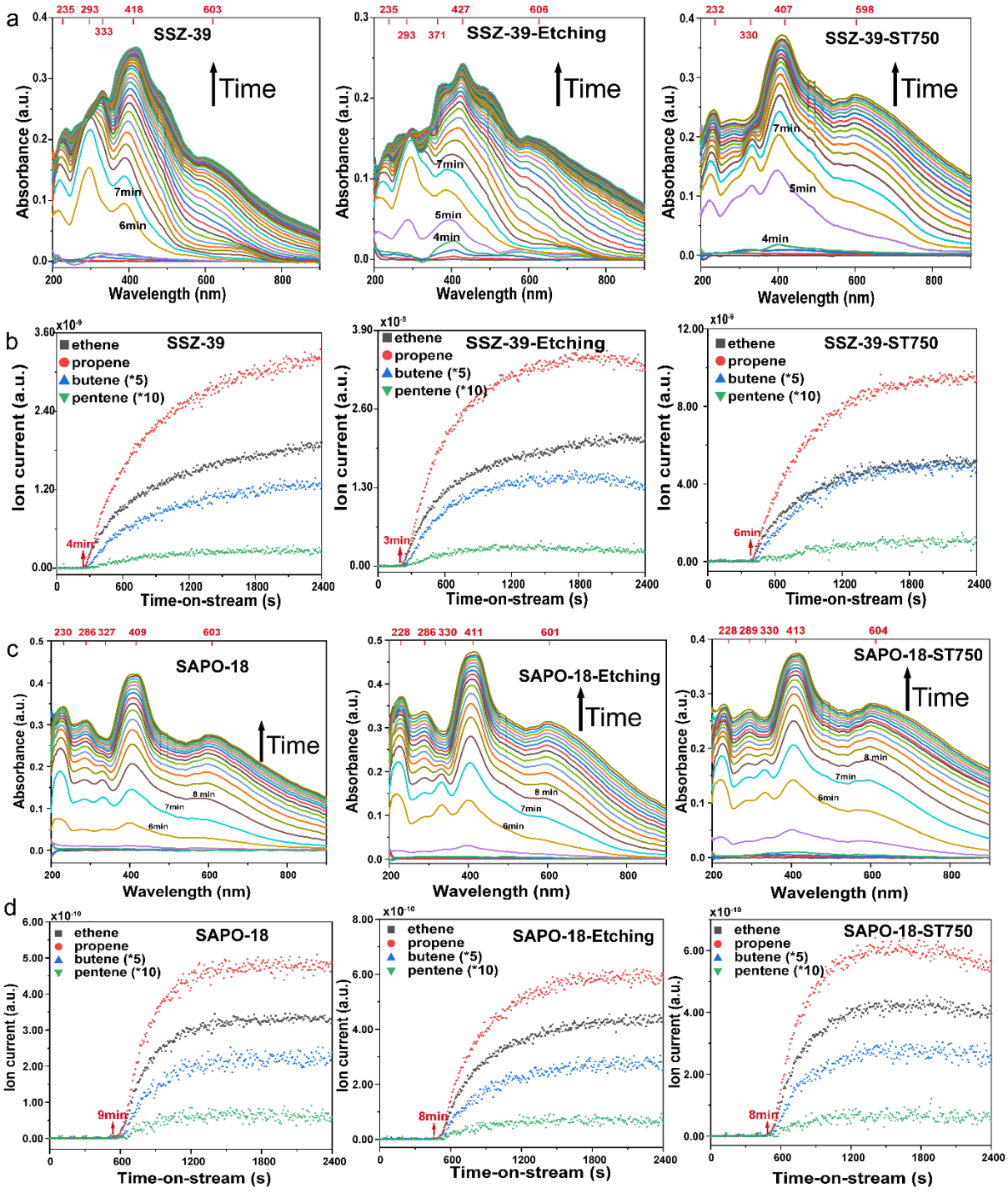

Fig. S19 The operando investigation of the MTO reaction over aluminosilicate SSZ-39 and SAPO-18 zeolites: the operando UV-vis profiles (a and c) and mass profiles (b and d) of methanol conversion, based on (a and b) (SSZ-39) and (c and d) (SAPO-18), at 400 °C for 40 min.

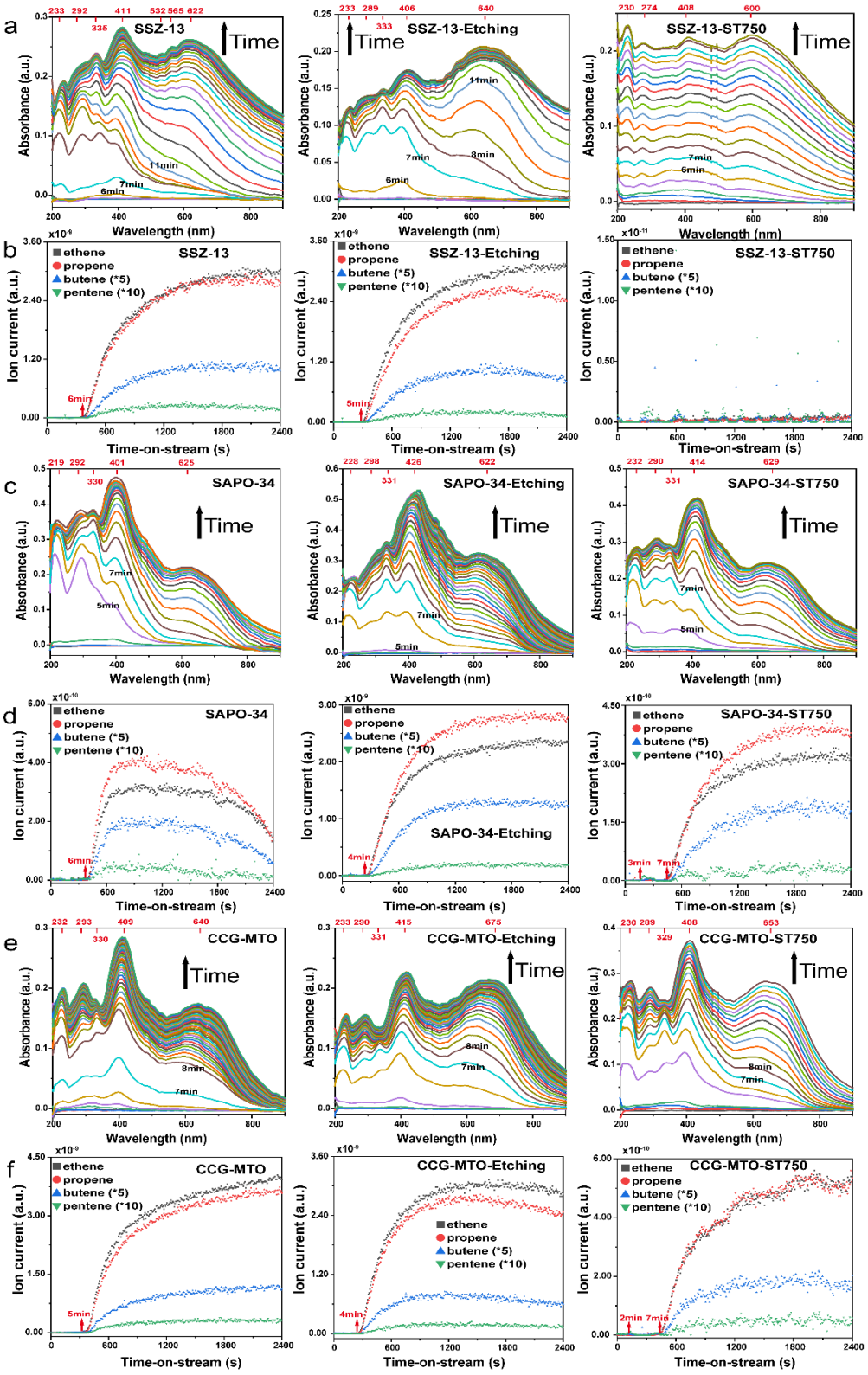

Fig. S20 The operando investigation of the MTO reaction over SSZ-13, SAPO-34 and CCG-MTO materials: the operando UV-vis profiles (a, c and e) and mass profiles (b,d and f) of methanol conversion, based on (a and b) (SSZ-13) , (c and d) (SAPO-34) and (e and f) (CCG-MTO) materials, at 400 °C for 40 min. (N.B.: MS-signals over SSZ-13-ST750 material remained weak in our different attempts, which could be due to product formation at a very low amount below the detection level of the instrument at the very early period of the reaction).

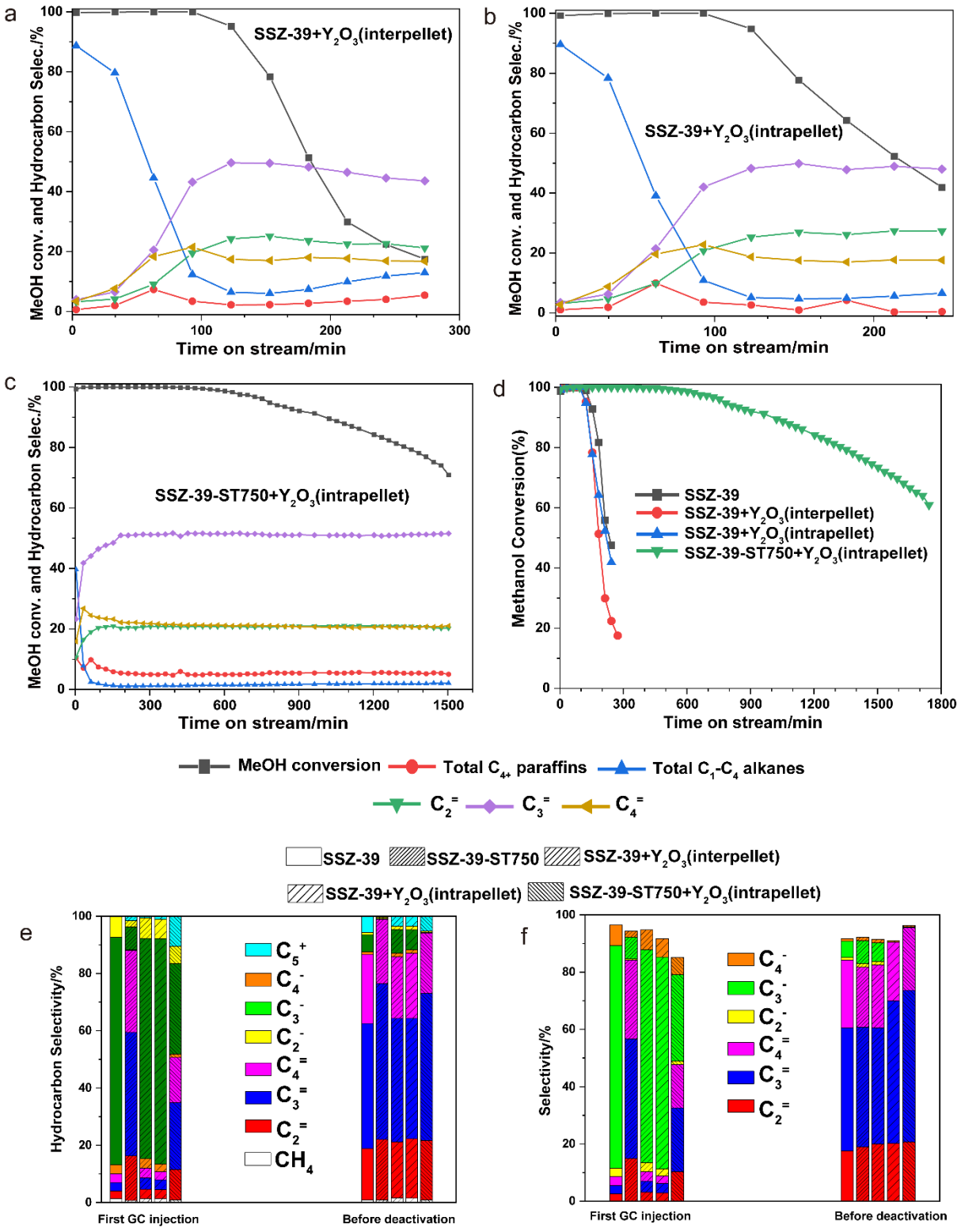

Fig. S21 Catalytic data of methanol conversion and hydrocarbon selectivity of the bifunctional catalytic system based on Y_2O_3 and SSZ-39 zeolites with respect to time-on-stream (TOS) (Reaction conditions:400 °C, WHSV=1h^{-1}): Bifunctional (a) SSZ-39-Interpellet, (b) SSZ-39-Intrapellet, and (c) SSZ-39-Intrapellet-ST750 materials. The overlapping comparison of their (d) Methanol conversion along with (e-f) hydrocarbon/product selectivity.

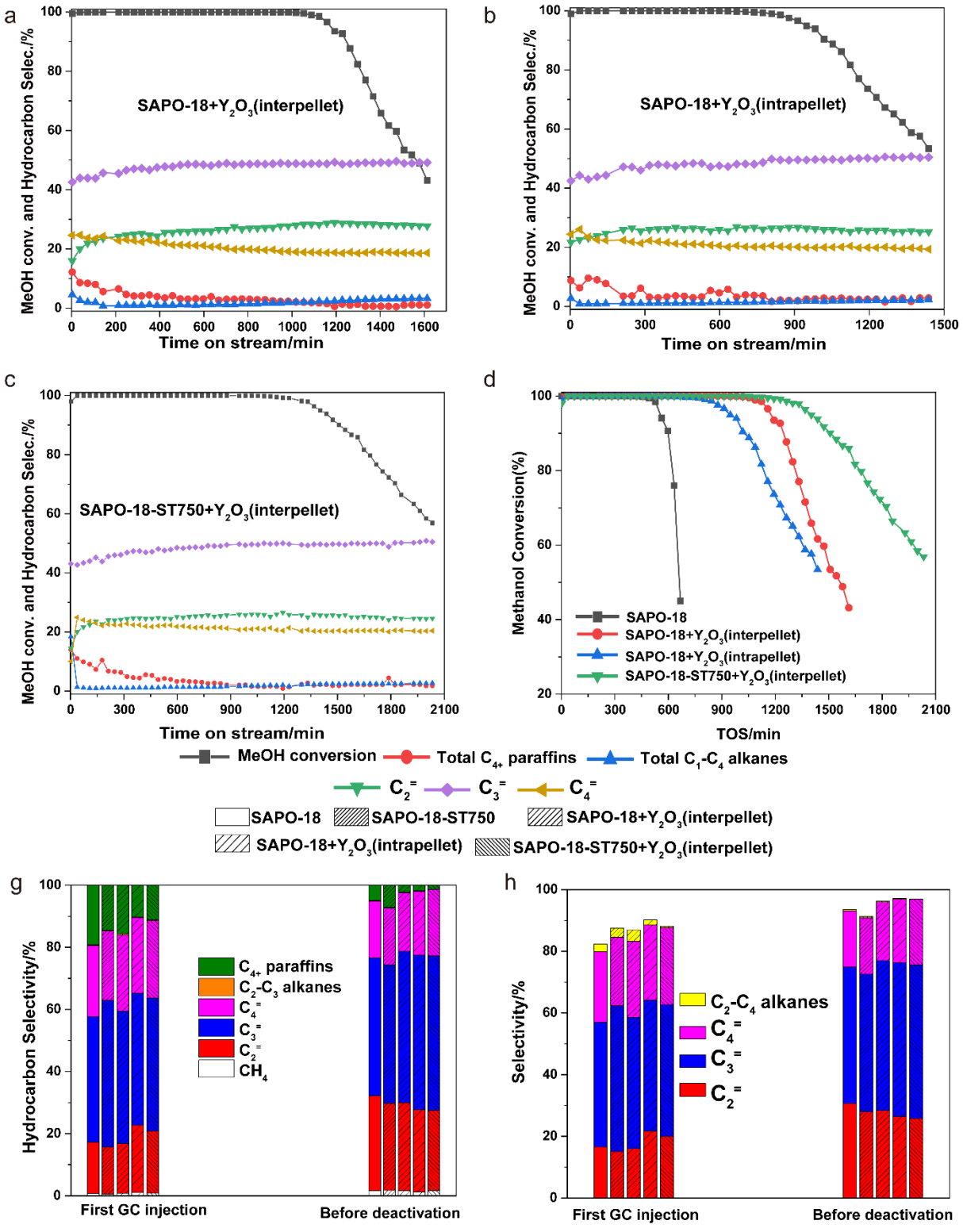

Fig. S22 Catalytic data of methanol conversion and hydrocarbon selectivity of the bifunctional catalytic system based on Y_2O_3 and SAPO-18 zeolites with respect to time-on-stream (TOS) (Reaction conditions:400 °C, WHSV=1h^{-1}): Bifunctional (a) SAPO-18-Interpellet, (b) SAPO-18-Intrapellet, and (c) SAPO-18-Interpellet-ST750 materials. The overlapping comparison of their (d) Methanol conversion along with (e-f) hydrocarbon/product selectivity.

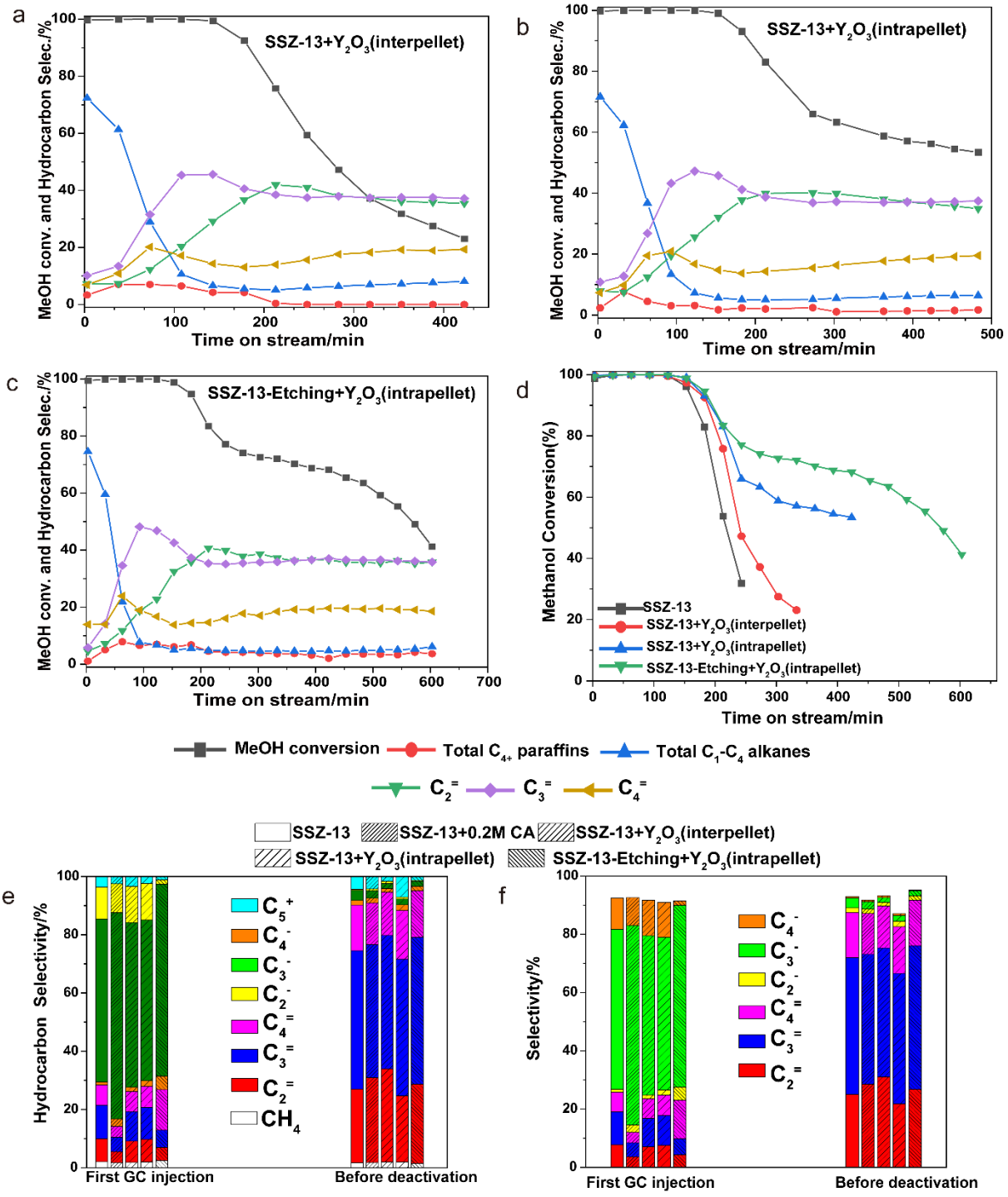

Fig. S23 Catalytic data of methanol conversion and hydrocarbon selectivity of the bifunctional catalytic system based on Y_2O_3 and SSZ-13 zeolites with respect to time-on-stream (TOS) (Reaction conditions:400 °C, WHSV=1h^{-1}): Bifunctional (a) SSZ-13-Interpellet, (b) SSZ-13-Intrapellet, and (c) SSZ-13-Intrapellet-0.2M CA materials (xM CA implies the citric acid concentration). The overlapping comparison of their (d) Methanol conversion along with (e-f) hydrocarbon/product selectivity.

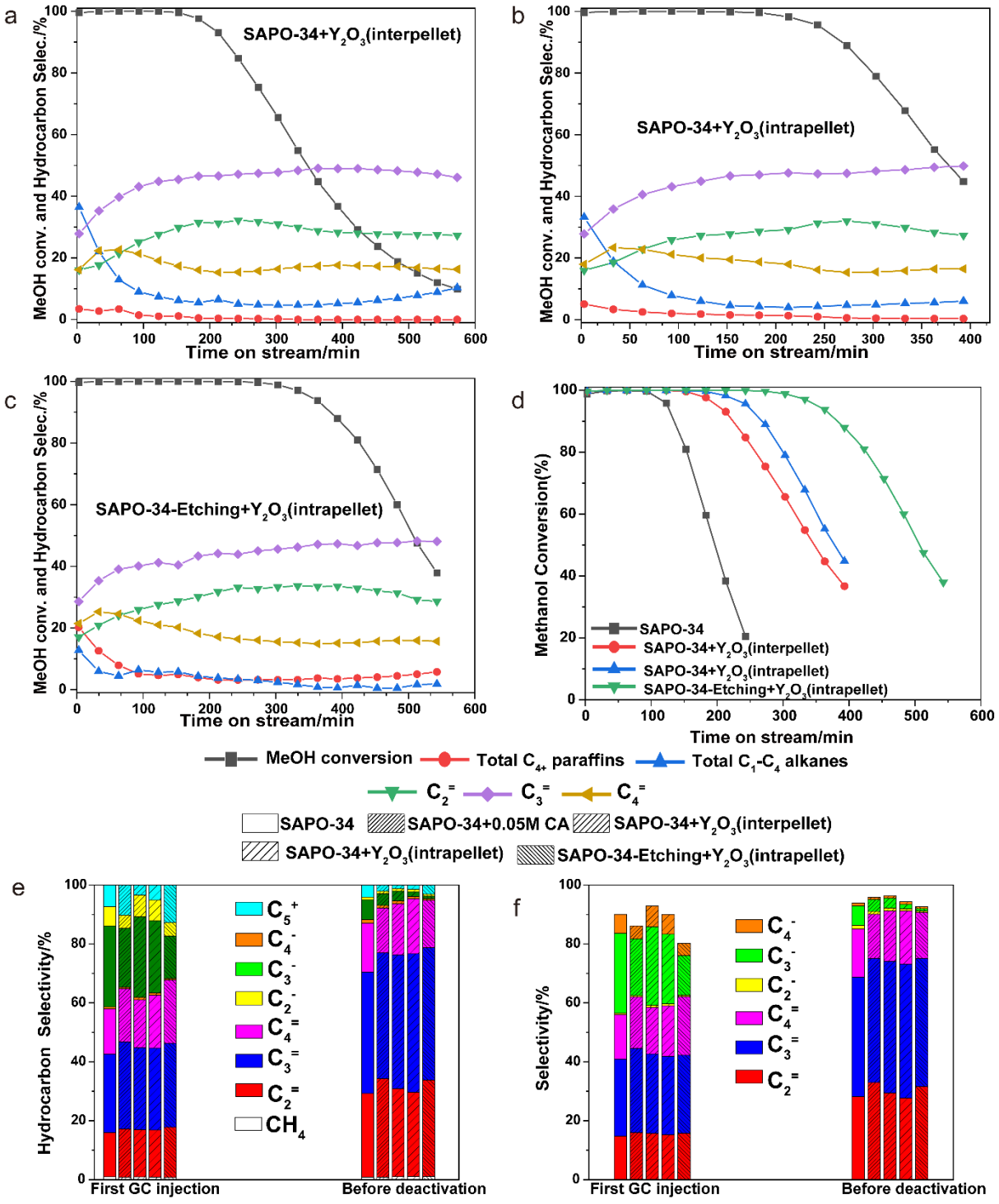

Fig. S24 Catalytic data of methanol conversion and hydrocarbon selectivity of the bifunctional catalytic system based on Y_2O_3 and SAPO-34 zeo-type materials with respect to time-on-stream (TOS) (Reaction conditions:400 °C, WHSV=1h^{-1}): Bifunctional (a) SAPO-34-Interpellet, (b) SAPO-34-Intrapellet, (c) SAPO-34-Intrapellet-0.05M CA materials (xM CA implies the citric acid concentration). The overlapping comparison of their (d) Methanol conversion along with (e-f) hydrocarbon/product selectivity.

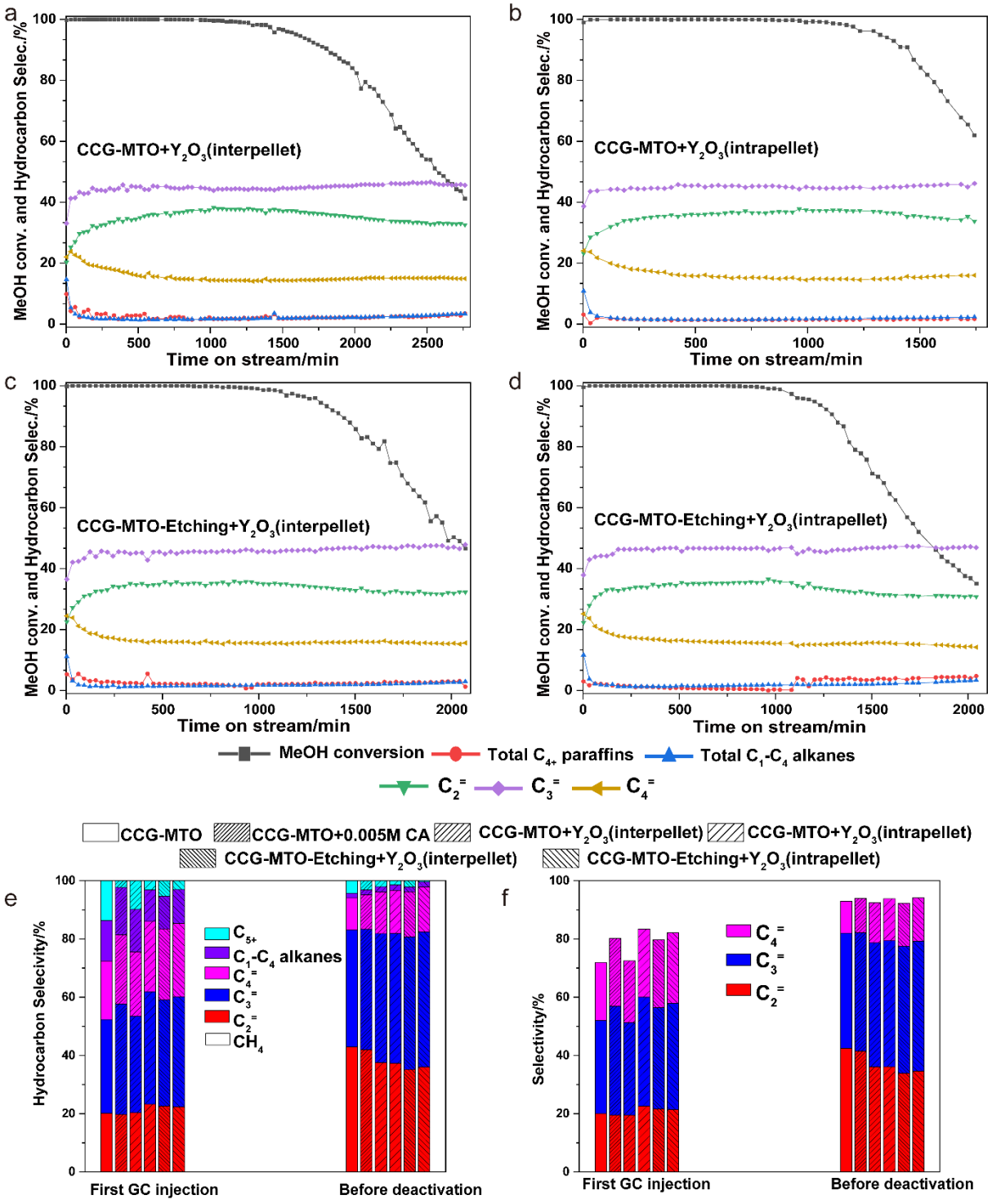

Fig. S25 Catalytic data of methanol conversion and hydrocarbon selectivity of the bifunctional catalytic system based on Y_2O_3 and CCG-MTO zeo-type materials with respect to time-on-stream (TOS) (Reaction conditions:400 °C, WHSV=1h^{-1}): Bifunctional (a) CCG-MTO-Interpellet, (b) CCG-MTO-Intrapellet, (c) CCG-MTO-Interpellet-0.005M CA, (d) CCG-MTO-Intrapellet-0.005M CA materials (xM CA implies the citric acid concentration). (e-f) The overlapping comparison of their hydrocarbon/product selectivity.

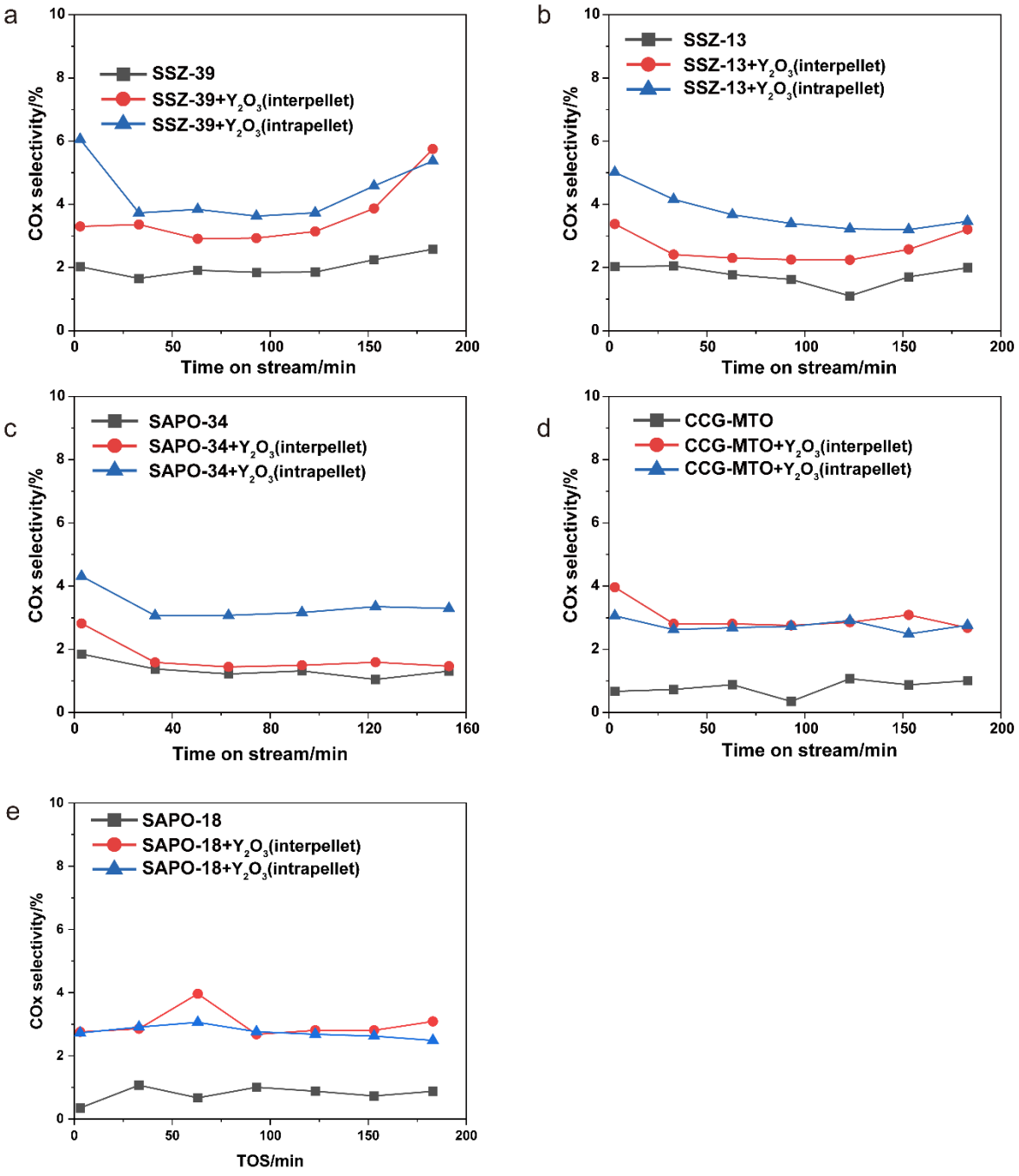

Fig. S26 CO_x(x=1,2) selectivity of over mono-and bifunctional (a) SSZ-39, (b) SSZ-13, (c) SAPO-34, and (d) CCG-MTO, and (e) SAPO-18 zeolite/zeo-type materials.

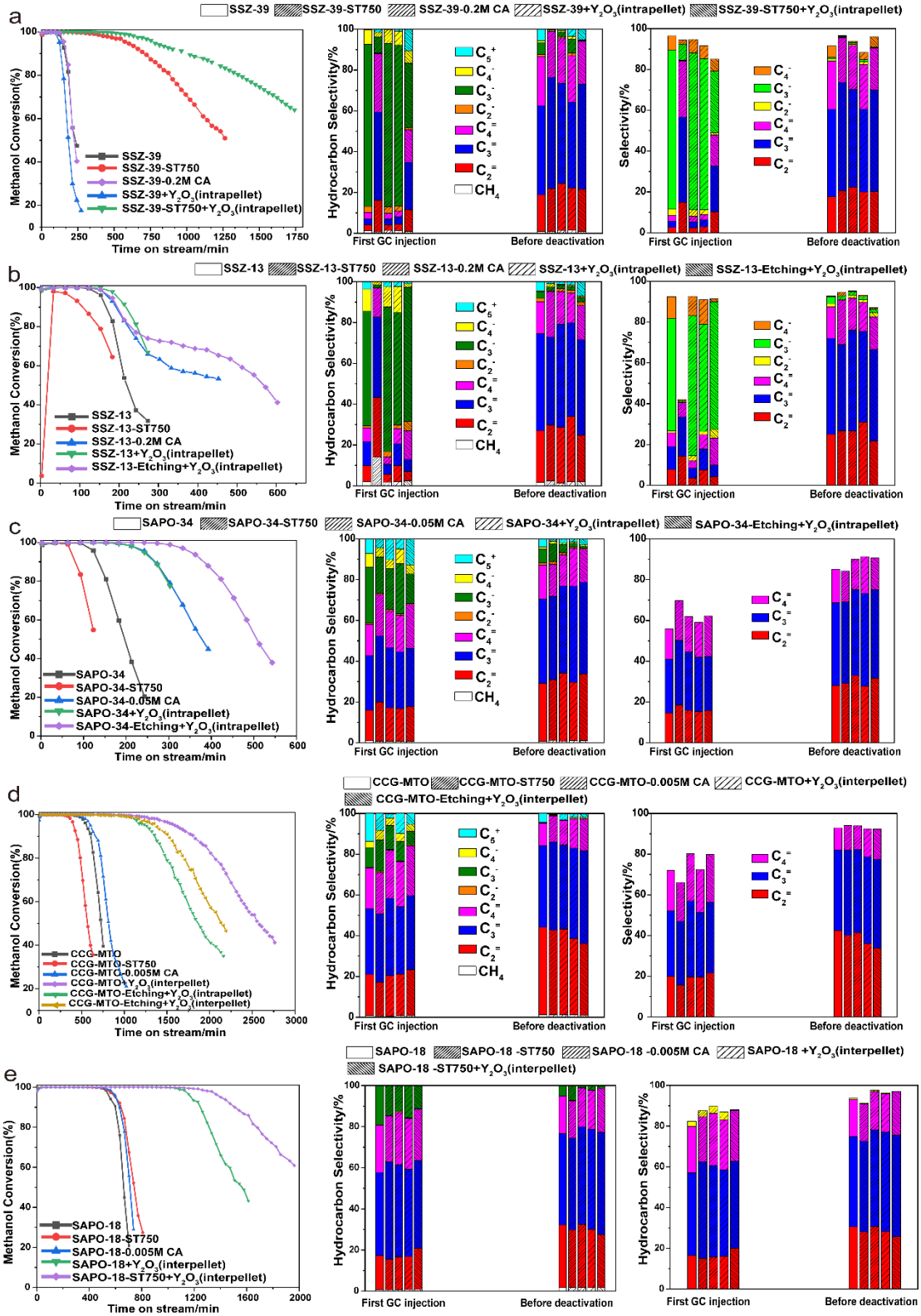

Fig. S27 The comparison profile of catalytic performance: Catalytic data of methanol conversion, and hydrocarbon/product selectivity over mono- and bifunctional catalytic system based on untreated and dealuminated (a) SSZ-39, (b) SSZ-13, (c) SAPO-34, and (d) CCG-MTO, (e) SAPO-18 zeolite/zeo-type materials (Reaction conditions:400 °C, WHSV=1h^{-1} and xM CA implies the citric acid concentration).

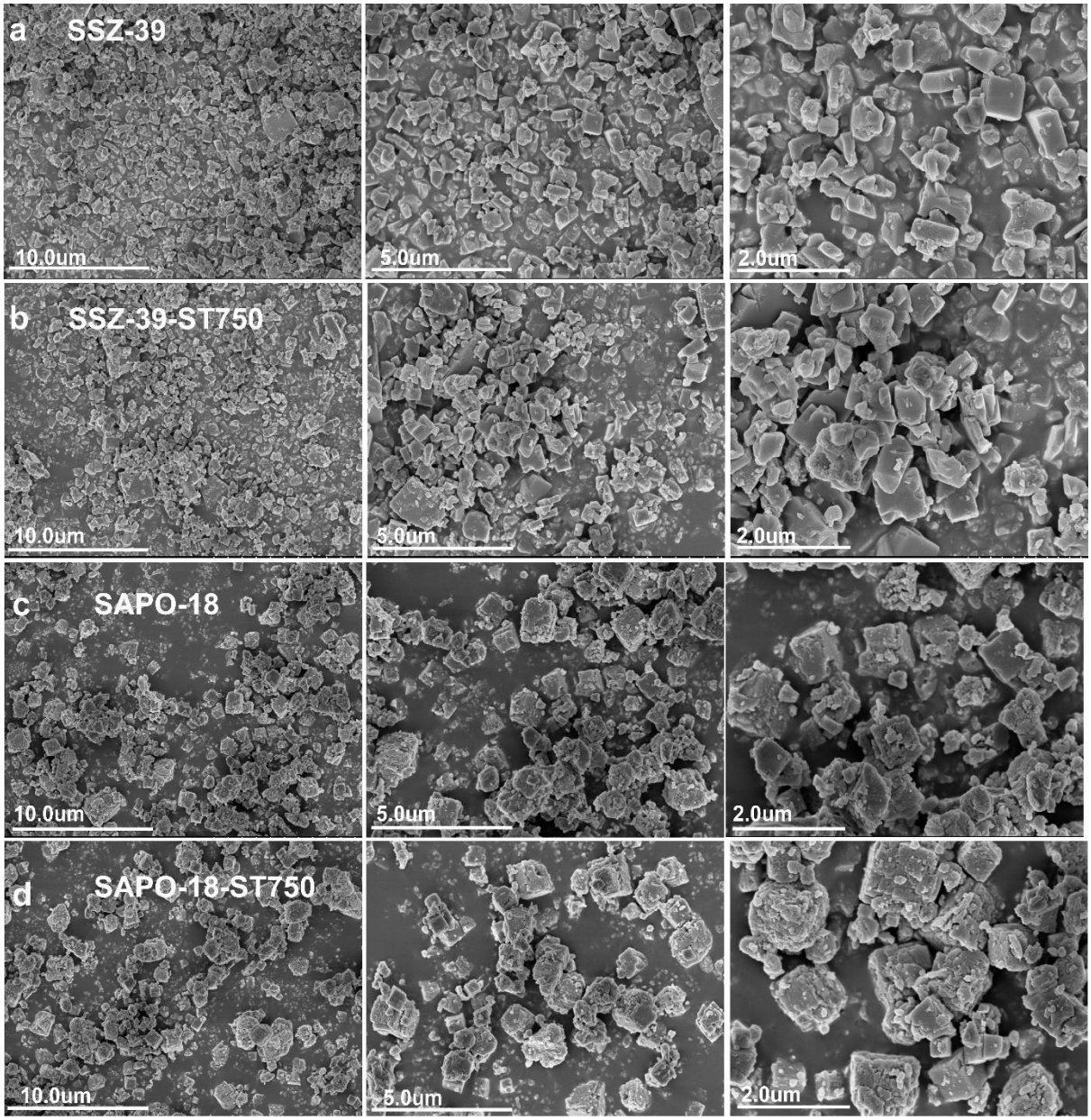

Fig. S28 SEM images of post-reacted (a) SSZ-39, (b) SSZ-39-ST750, (c) SAPO-18, (d) SAPO-18-ST750 zeolites.

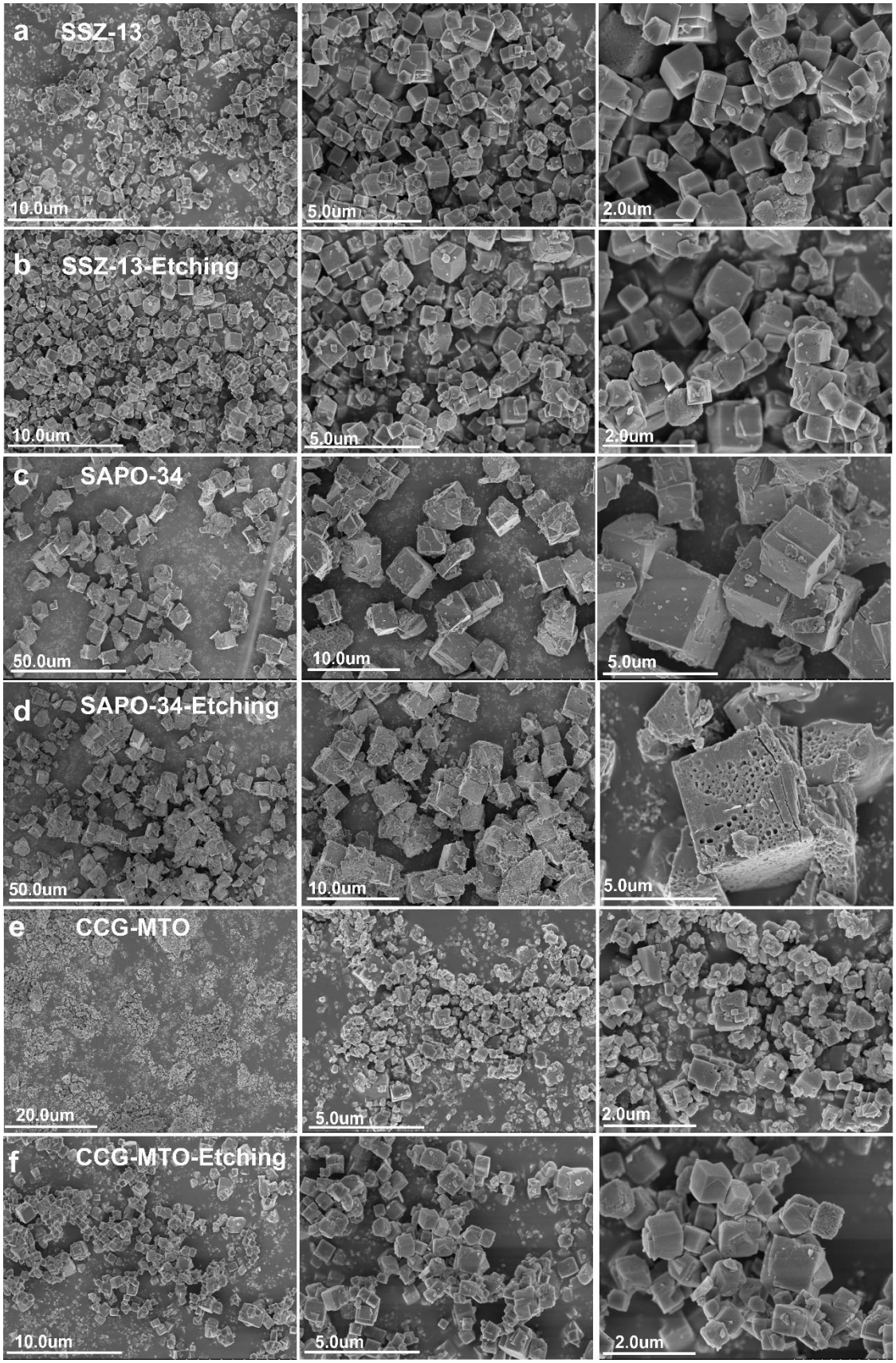

Fig. S29 SEM images of post-reacted (a) SSZ-13, (b) SSZ-13-Etching, (c) SAPO-34, (d) SAPO-34-Etching, (e) CCG-MTO, and (f) CCG-MTO-Etching zeolite/zeo-type materials.

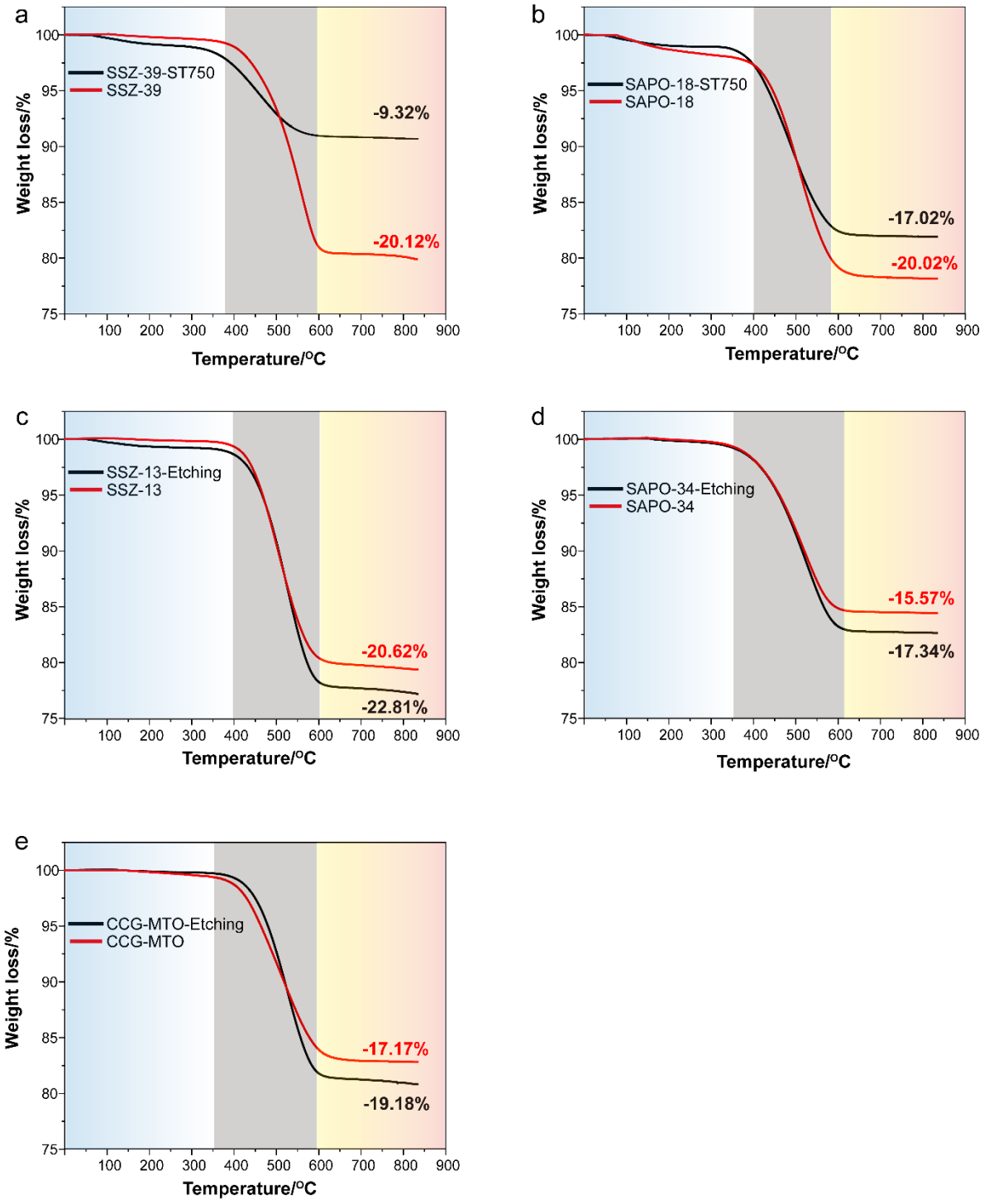

Fig. S30 TGA study of spent zeolite catalysts obtained after MTO catalytic testing: (a) SSZ-39 and SSZ-39-ST750 zeolites; (b) SAPO-18 and SAPO-18-ST750 zeolites; (c) SSZ-13 and SSZ-13-Etching zeolites; (d) SAPO-34 and SAPO-34-Etching zeolites; (e) CCG-MTO and CCG-MTO-Etching zeo-type materials. These spent and deactivated zeolite catalysts were heated from room temperature to 850 °C at a rate of 10 °C/min in an airflow of 30 ml/min. The

aromatics-based coke species were typically removed in an air atmosphere within the temperature range of 300 to 700 °C. The TGA measurements of spent catalysts were performed under flowing air, revealing two distinct weight loss steps: the first attributed to water adsorption before 300 °C, and the second related to coke decomposition between 400 °C and 700 °C.[11–13] Interestingly, comparable water weight loss was observed for both the 8-MR parent zeolite and the optimal dealuminated sample. However, for SSZ-39 and SAPO-18 zeolites, the parent zeolite exhibited higher coke deposition compared to samples treated with steam dealumination. Conversely, regarding SSZ-13, SAPO-18, and CCG-MTO zeo/zeo-type materials, the parent zeolite showed lower weight loss compared to samples treated with citric acid etching, indicating an increase in coke capacity for the etched zeolites, thereby prolonging their lifespan.[11–13] UV-vis analysis revealed that CCG-MTO exhibits a slower rate of absorption increase above 500 nm compared to SAPO-34, indicating its high coke capacity. TGA analysis of post-reaction zeolite shows a carbon deposition of 17.17% for CCG-MTO and 15.57% for SAPO-34, highlighting that CCG-MTO material has superior carbon volumetric capacity. Furthermore, CCG-MTO accumulates more coke precursors, evidenced by higher intensity >550 nm bands related to poly-aromatic coke precursors. Steamed SSZ-39 and SAPO-18 demonstrate a slower rise in relevant UV-vis bands and superior catalyst lifetime. Chemically etched SSZ-13, SAPO-34, and CCG-MTO zeo/zeo-type materials exhibit a slower rise in relevant UV-vis bands and superior catalyst lifetime, as indicated by TGA analysis showing high carbon capacity and prominent weight loss peaks.

Table S1 Shorter olefins selectivity[a] of MTO reaction performed over both mono- and bifunctional catalytic system, that also includes both parent/untreated and dealuminated zeolite/zeo-type materials reaction.

Materials	$t_{80\%}$[a] (min)	$C_2^=$(%)[b]	$C_3^=$(%)[b]	$C_4^=$(%)[b]	$C_2^=$-$C_4^=$(%)[b]
SSZ-39	~180	18	44	24	86
SSZ-39-Etching	~180	23	49	22	94
SSZ-39-ST750	~870	21	54	23	98
SSZ-39+Y_2O_3 (interpellet)	~150	19	43	22	84
SSZ-39+Y_2O_3 (intrapellet)	~150	21	42	23	86
SSZ-39-ST750+Y_2O_3 (intrapellet)	~1300	21	51	21	93
SAPO-18	~600	31	44	18	93
SAPO-18-Etching	~660	31	47	19	97
SAPO-18-ST750	~700	28	45	18	91
SAPO-18+Y_2O_3 (interpellet)	~1300	28	49	19	96
SAPO-18+Y_2O_3 (intrapellet)	~1150	26	50	21	97
SAPO-18-ST750+Y_2O_3 (interpellet)	~1650	26	50	21	97
SSZ-13	~180	25	47	16	88
SSZ-13-Etching	~240	27	50	16	93
SSZ-13-ST750	~150	27	43	22	92
SSZ-13+Y_2O_3 (interpellet)	~210	29	46	14.	89
SSZ-13+Y_2O_3 (intrapellet)	~240	32	46	15	93
SSZ-13-Etching+Y_2O_3 (intrapellet)	~240	23	47	17	87
SAPO-34	~150	28	41	17	86
SAPO-34-Etching	~300	33	43	15	91
SAPO-34-ST750	~100	30	41	16	87
SAPO-34+Y_2O_3 (interpellet)	~240	30	45	17	92
SAPO-34+Y_2O_3 (intrapellet)	~300	29	47	19	95
SAPO-34-Etching+Y_2O_3 (intrapellet)	~420	33	45	16	94
CCG-MTO	~630	43	40	11	94
CCG-MTO-Etching	~690	42	41	12	95
CCG-MTO-ST750	~500	42	43	12	97
CCG-MTO+Y_2O_3 (interpellet)	~2000	37	44	14	95
CCG-MTO+Y_2O_3 (intrapellet)	~1500	37	45	15	97
CCG-MTO-Etching+Y_2O_3 (interpellet)	~1600	35	45	16	96
CCG-MTO-Etching+Y_2O_3 (intrapellet)	~1400	36	46	15	97

[a] Based on the methanol conversion till ≥ 80%.

[b] Based on the average selectivity of $C_2^=$,$C_3^=$,$C_4^=$ under > 99% methanol conversion.

Table S2: Chemical composition of parent and dealuminated zeolites/zeo-type materials obtained from XRF (X-Ray Fluorescence).

Metal oxide analysis (weight %)						
Samples	***SiO_2***	***Al_2O_3***	***P_2O_5***	***Na_2O***	***SiO_2/Al_2O_3[a]***	
SSZ-39	*89.92*	*10.01*	*0.01*	*0.06*	*15.2*	
SSZ-39-Etching	*89.63*	*9.93*	*0.04*	*--*	*15.3*	
SSZ-39-ST750	*90.16*	*9.66*	*0.04*	*0.08*	*15.8*	
SAPO-18	*5.11*	*53.02*	*41.63*	*0.07*	*0.2*	
SAPO-18-Etching	*4.67*	*53.35*	*41.88*	*--*	*0.1*	
SAPO-18-ST750	*4.9*	*52.02*	*42.84*	*0.05*	*0.2*	
SSZ-13	*93.15*	*6.84*	*--*	*0.01*	*23.1*	
SSZ-13-Etching	*93.02*	*6.68*	*0.01*	*0.02*	*23.6*	
SSZ-13-ST750	*93.41*	*6.51*	*0.02*	*0.01*	*24.3*	
SAPO-34	*9.93*	*47.94*	*42.17*	*--*	*0.4*	
SAPO-34-Etching	*8.95*	*48.75*	*42.31*	*--*	*0.3*	
SAPO-34-ST750	*9.83*	*47.14*	*42.97*	*--*	*0.4*	
CCG-MTO	*5.31*	*49.09*	*45.52*	*--*	*0.2*	
CCG-MTO-Etching	*4.92*	*49.39*	*45.59*	*--*	*0.2*	
CCG-MTO-ST750	*5.15*	*47.95*	*46.97*	*--*	*0.2*	
Elemental analysis (weight %)						
Samples	***Si***	***Al***	***P***	***Na***	***Si/Al[a]***	***(Si+P)/Al[a]***
SSZ-39	*42.03*	*5.30*	*0.00*	*0.03*	*7.6*	*--*
SSZ-39-Etching	*41.90*	*5.26*	*0.02*	*0.00*	*7.7*	*--*
SSZ-39-ST750	*42.14*	*5.11*	*0.02*	*0.04*	*7.9*	*--*
SAPO-18	*2.39*	*28.06*	*18.17*	*0.03*	*--*	*0.64*
SAPO-18-Etching	*2.18*	*28.24*	*18.28*	*0.00*	*--*	*0.63*
SAPO-18-ST750	*2.29*	*27.53*	*18.70*	*0.02*	*--*	*0.67*
SSZ-13	*43.54*	*3.62*	*0.00*	*0.00*	*11.6*	*--*
SSZ-13-Etching	*43.48*	*3.54*	*0.00*	*0.01*	*11.8*	*--*
SSZ-13-ST750	*43.66*	*3.45*	*0.01*	*0.00*	*12.2*	*--*
SAPO-34	*4.64*	*25.37*	*18.40*	*0.00*	*--*	*0.80*
SAPO-34-Etching	*4.18*	*25.80*	*18.46*	*0.00*	*--*	*0.77*
SAPO-34-ST750	*4.59*	*24.95*	*18.75*	*0.00*	*--*	*0.83*
CCG-MTO	*2.48*	*25.98*	*19.87*	*0.00*	*--*	*0.75*
CCG-MTO-Etching	*2.30*	*26.14*	*19.90*	*0.00*	*--*	*0.74*
CCG-MTO-ST750	*2.41*	*25.38*	*20.50*	*0.00*	*--*	*0.79*

[a]molar ratio. These findings indicate a consistent reduction in bulk phase aluminum content for aluminosilicate zeolites (SSZ-39 and SSZ-13) following both chemical etching and steamed

treatment, with the severity of treatment correlating positively with the Si/Al ratio, consistent with previous studies.[4,12,14–17] The Si/Al ratios of etched and steamed samples (Table S2) closely mirrored those of the initial CHA, with the minimal variance within the margin of measurement error. In the case of aluminophosphate (ALPO) zeolites (SAPO-18, SAPO-34, and CCG-MTO), citric acid etching resulted in a sequential loss of Si > Al > P in the bulk phase, accompanied by a diminishing trend in (Si+P)/Al ratio. This trend suggests the selective removal of isolated Si(4Al) and Si islands from the framework post-acid treatment. Conversely, steam-treated aluminophosphate zeolites exhibited an upward trend in (Si+P)/Al, consistent with prior research.[1,4,12,14–16] Further elucidation of variations in the silicon-to-aluminum ratio and a deeper understanding of dealumination and desilication mechanisms warrant additional comprehensive analyses, which will be pursued in subsequent investigations.

Table S3 Summary of acidic properties of untreated and dealuminated zeolite/zeo-type materials used.

Samples	**Weak[a] /mmolg^{-1}**	**Medium [a] /mmolg^{-1}**	**Strong[a] /mmolg^{-1}**	**Total[a] /mmolg^{-1}**	**Strong /Weak**	**Strong /Total**
SSZ-39	0.55	-	0.36	0.91	0.65	0.40
SSZ-39-Etching	0.56	-	0.33	0.89	0.59	0.37
SSZ-39-ST750	0.24	0.41	0.10	0.75	0.42	0.13
SAPO-18	0.25	--	0.40	0.65	1.60	0.62
SAPO-18-Etching	0.32	--	0.29	0.61	0.91	0.48
SAPO-18-ST750	0.40	0.10	0.09	0.59	0.23	0.15
SSZ-13	0.73	-	0.39	1.12	0.53	0.35
SSZ-13-Etching	0.25	0.51	0.17	0.93	0.68	0.18
SSZ-13-ST750	0.27	0.54	0.05	0.86	0.19	0.06
SAPO-34	0.28	-	0.26	0.54	0.93	0.48
SAPO-34-Etching	0.28	-	0.21	0.49	0.75	0.43
SAPO-34-ST750	0.31	-	0.11	0.42	0.35	0.26
CCG-MTO	0.15	-	0.26	0.41	1.73	0.63
CCG-MTO-Etching	0.26	-	0.15	0.41	0.58	0.37
CCG-MTO-ST750	0.18	0.10	0.09	0.37	0.50	0.24

[a]Acidity distribution of treated and untreated zeolites by NH_3-TPD.

Supplementary References

1 T. Zheng, H. Liu, P. He, R. Zhang, X. Meng, C. Xu, H. Liu, Y. Yue and Z. Liu, *Microporous and Mesoporous Materials*, 2022, **335**, 111798.

2 V. Babić, S. Koneti, S. Moldovan, N. Nesterenko, J. P. Gilson and V. Valtchev, *Microporous and Mesoporous Materials*, 2021, **314**, 110863.

3 W. Jin, B. Wang, P. Tuo, C. Li, L. Li, H. Zhao, X. Gao and B. Shen, *Ind Eng Chem Res*, 2018, **57**, 4231–4236.

4 L. Sommer, D. Mores, S. Svelle, M. Stöcker, B. M. Weckhuysen and U. Olsbye, *Microporous and Mesoporous Materials*, 2010, **132**, 384–394.

5 M. Dusselier, M. A. Deimund, J. E. Schmidt and M. E. Davis, *ACS Catal*, 2015, **5**, 6078–6085.

6 M. A. Deimund, L. Harrison, J. D. Lunn, Y. Liu, A. Malek, R. Shayib and M. E. Davis, *ACS Catal*, 2016, **6**, 542–550.

7 A. P. Hawkins, A. Zachariou, S. F. Parker, P. Collier, N. Barrow, I. P. Silverwood, R. F. Howe and D. Lennon, *RSC Adv*, 2020, **10**, 23136–23147.

8 Z. Xu, J. Li, Y. Huang, H. Ma, W. Qian, H. Zhang and W. Ying, *Catal Commun*, 2020, **141**, 1–7.

9 A. Hwang and A. Bhan, *ACS Catal*, 2017, **7**, 4417–4422.

10 Y. Wang, S. L. Chen, Y. L. Gao, Y. Q. Cao, Q. Zhang, W. K. Chang and J. B. Benziger, *ACS Catal*, 2017, **7**, 5572–5584.

11 S. Ren, G. Liu, X. Wu, X. Chen, M. Wu, G. Zeng, Z. Liu and Y. Sun, *Chinese Journal of Catalysis*, 2017, **38**, 123–130.

12 W. Dai, G. Wu, L. Li, N. Guan and M. Hunger, *ACS Catal*, 2013, **3**, 588–596.

13 W. Dai, M. Scheibe, N. Guan, L. Li and M. Hunger, *ChemCatChem*, 2011, **3**, 1130–1133.

14 V. Babić, S. Koneti, S. Moldovan, N. Nesterenko, J. P. Gilson and V. Valtchev, *Microporous and Mesoporous Materials*, 2021, **314**, 110863.

15 R. Oord, I. C. Ten Have, J. M. Arends, F. C. Hendriks, J. Schmidt, I. Lezcano-Gonzalez and B. M. Weckhuysen, *Catal Sci Technol*, 2017, **7**, 3851–3862.

16 W. Jin, B. Wang, P. Tuo, C. Li, L. Li, H. Zhao, X. Gao and B. Shen, *Ind Eng Chem Res*, 2018, **57**, 4231–4236.

17 D. Fan, Y. Qiao, K. Cao, L. Sun, S. Xu, P. Tian and Z. Liu, *Microporous and Mesoporous Materials*, , DOI:10.1016/j.micromeso.2020.110156.